Cell Reports
Medicine

Article

Deficiency of the CD155-CD96 immune checkpoint controls IL-9 production in giant cell arteritis

Graphical abstract

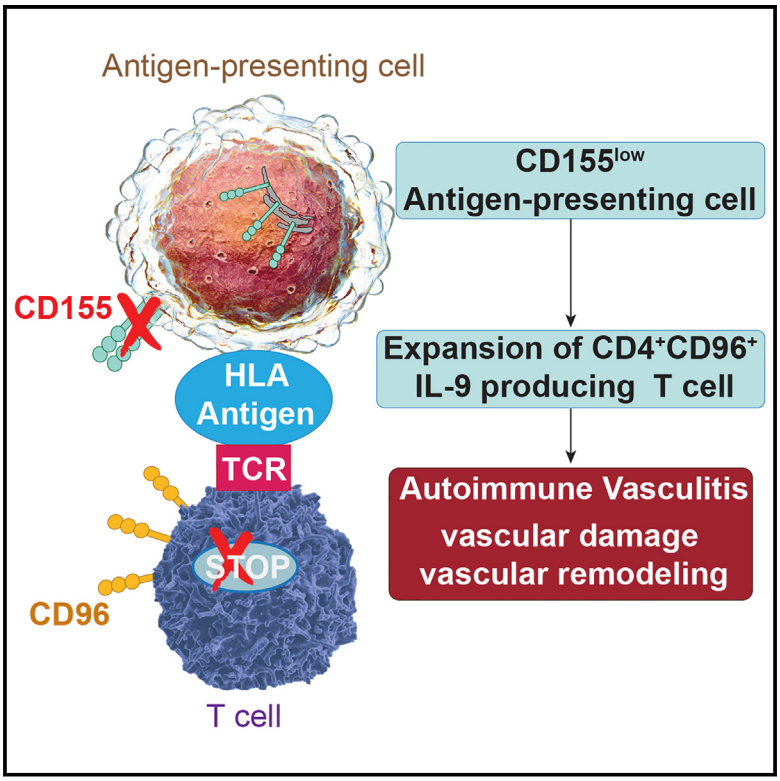

Authors

Shozo Ohtsuki, Chenyao Wang, Ryu Watanabe, ..., Gerald J. Berry, Jörg J. Goronzy, Cornelia M. Weyand

Correspondence

cweyand@stanford.edu

In brief

Ohtsuki et al. report that patients with the autoimmune vasculitis giant cell arteritis (GCA) have a tolerance defect caused by the loss of an inhibitory immune checkpoint. CD155^{low}-expressing antigen-presenting cells drive expansion of CD4^{+}CD96^{+} T cells that produce the cytokine IL-9. Blocking IL-9 has therapeutic efficacy in experimental vasculitis.

Highlights

- Patients with giant cell arteritis have a defective CD155-CD96 immune checkpoint
- Antigen-presenting cells (APCs) retain CD155 in the endoplasmic reticulum
- CD155^{low} APCs favor the differentiation of IL-9-producing CD4^{+}CD96^{+} memory T cells
- IL-9 drives tissue-damaging immunity in vasculitis

Ohtsuki et al., 2023, Cell Reports Medicine *4*, 101012
April 18, 2023
https://doi.org/10.1016/j.xcrm.2023.101012

CellPress

Cell Reports Medicine

CellPress
OPEN ACCESS

Article

Deficiency of the CD155-CD96 immune checkpoint controls IL-9 production in giant cell arteritis

Shozo Ohtsuki,[1,2,3,4] Chenyao Wang,[2,3,4] Ryu Watanabe,[1,5] Hui Zhang,[1,6] Mitsuhiro Akiyama,[1,7] Melanie C. Bois,[8] Joseph J. Maleszewski,[8] Kenneth J. Warrington,[2] Gerald J. Berry,[9] Jörg J. Goronzy,[1,2,4] and Cornelia M. Weyand[1,2,3,4,10,*]

[1]Department of Medicine, School of Medicine, Stanford University, Stanford, CA 94305, USA
[2]Department of Medicine, Mayo Clinic College of Medicine and Science, Rochester, MN 55905, USA
[3]Department of Cardiology, Mayo Clinic College of Medicine and Science, Rochester, MN 55905, USA
[4]Department of Immunology, Mayo Clinic College of Medicine and Science, Rochester, MN 55905, USA
[5]Department of Clinical Immunology, Osaka Metropolitan University Graduate School of Medicine, Osaka, Japan
[6]Deptartment of Rheumatology, Institute of Precision Medicine, The First Affiliated Hospital, Sun Yat-sen University, Guangdong, China
[7]Division of Rheumatology, Department of Internal Medicine, Keio University School of Medicine, Tokyo, Japan
[8]Department of Laboratory Medicine and Pathology, Mayo Clinic, Rochester, MN 55905, USA
[9]Department of Pathology, School of Medicine, Stanford University, Stanford, CA 94305, USA
[10]Lead contact
*Correspondence: cweyand@stanford.edu
https://doi.org/10.1016/j.xcrm.2023.101012

SUMMARY

Loss of function of inhibitory immune checkpoints, unleashing pathogenic immune responses, is a potential risk factor for autoimmune disease. Here, we report that patients with the autoimmune vasculitis giant cell arteritis (GCA) have a defective CD155-CD96 immune checkpoint. Macrophages from patients with GCA retain the checkpoint ligand CD155 in the endoplasmic reticulum (ER) and fail to bring it to the cell surface. $CD155^{low}$ antigen-presenting cells induce expansion of $CD4^+CD96^+$ T cells, which become tissue invasive, accumulate in the blood vessel wall, and release the effector cytokine interleukin-9 (IL-9). In a humanized mouse model of GCA, recombinant human IL-9 causes vessel wall destruction, whereas anti-IL-9 antibodies efficiently suppress innate and adaptive immunity in the vasculitic lesions. Thus, defective surface translocation of CD155 creates antigen-presenting cells that deviate T cell differentiation toward Th9 lineage commitment and results in the expansion of vasculitogenic effector T cells.

INTRODUCTION

Immune checkpoint receptor/ligand pairs critically control the kinetics, duration, and intensity of immune responses, as exemplified by the high expression of checkpoint ligands on tumor cells that enable tumor immune evasion.[1–3] Immune checkpoint blockade has revolutionized cancer therapy but also causes immune-related adverse events (irAEs), often mimicking autoimmune disease.[4] Accordingly, inherited or acquired deficiency of suppressive checkpoints may have relevance in spontaneous autoimmunity. In support of this concept, patients with the autoimmune vasculitis giant cell arteritis (GCA) have low expression of the checkpoint ligand PD-L1 on antigen-presenting cells (APCs), and blockade of the PD-1/PD-L1 checkpoint exacerbates arteritis.[5]

GCA is an autoimmune vasculitis of medium and large arteries, frequently involving the aorta. Disease hallmarks include granulomatous infiltrates in the vessel wall, typically associated with multinucleated giant cells.[6] Vascular infiltrates contain $CD4^+$ T cells and highly activated macrophages (Mφs),[7] and the vessel wall reacts with a maladaptive response to injury, forming lumen-occlusive intimal hyperplasia.[8] Aberrantly expressed NOTCH1 receptors on $CD4^+$ T cells enhance co-stimulatory signaling and foster T cell transmigration from vasa vasora into the vascular wall through NOTCH-Jagged interactions.[9] Lesional T cells produce an array of effector cytokines, including interferon-γ (IFN-γ), interleukin-2 (IL-2), IL-22, and IL-9.[10,11] Loss of self-tolerance has been attributed to the loss of immunoinhibitory T regulatory cells, which release NADPH-containing exosomes to inhibit neighboring $CD4^+$ T cells.[12] Age is an established risk factor with disease onset consistently after the age of 50 years[13] Based on serial biopsy studies, many patients have refractory vasculitis with persistent inflammation despite immunosuppressive therapy.[14]

Given the granulomatous character of GCA, Mφs are key contributors to the disease process.[15] Circulating monocytes overexpress MMP-9 and digest basal membranes to get access to the adventitial space.[16] GCA Mφs produce chemokines and cytokines, have comparably low metabolic activity,[17] and express low density of PD-L1, thus functioning as "permissive" APCs.[5] Accordingly, the disease process relies on CD80/CD86-dependent co-stimulation to build tissue-damaging infiltrates that trigger neoangiogenesis and wall remodeling.[8] Wall-residing Mφs participate in the handling of oxidative stress[17] and supply growth and angiogenesis factors[18] that mediate immune-mediated vascular restructuring.

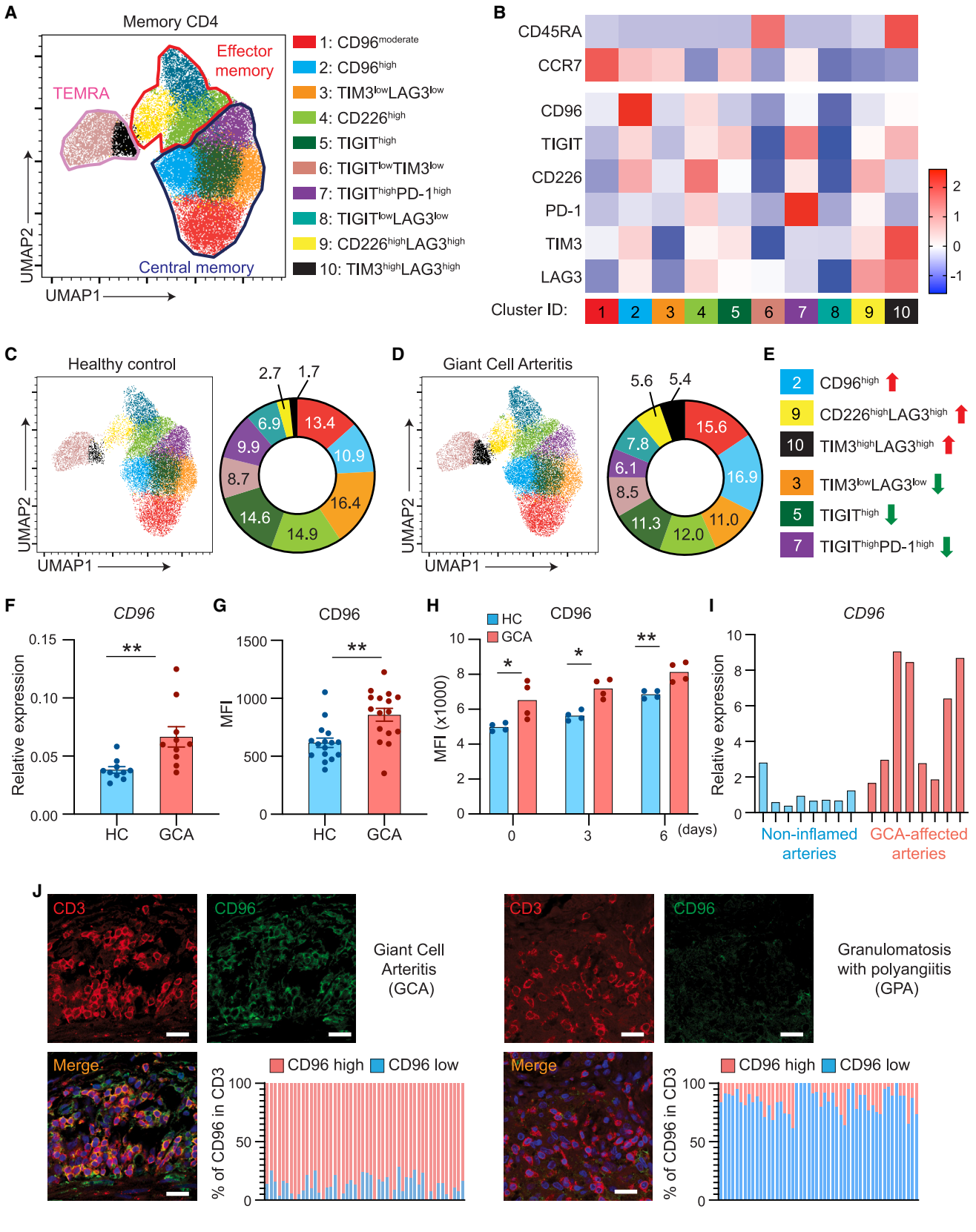

(legend on next page)

Comparative studies between atherosclerosis and GCA have been informative in linking immune cell phenotype to function and disease.[17] Glucose is a dominant energy source for Mφs in coronary artery disease, fueling high mitochondrial activity,[17] cytokine secretion,[19] and high PD-L1 expression.[17] Mφs accumulating in atherosclerotic lesions express high amounts of the checkpoint ligand CD155,[20] and a hyperactive CD155 immune checkpoint impairs the host's anti-viral immunity. Overall, atherosclerotic lesions recruit and retain Mφs displaying immunosuppressive functions, contrasting the "permissive" Mφs associated with GCA.

The transmembrane glycoprotein CD155, also known as the poliovirus receptor (PVR), is a member of the immunoglobulin superfamily and regulates natural killer (NK) adhesion and effector functions.[21] CD155 is expressed on monocytes, dendritic cells, and tumor cells, where it provides a negative signal and functions as a classical immunoinhibitory ligand. CD155 binds to the CD96, TIGIT, and CD226 surface receptors on T cells and NK cells. CD96 and TIGIT are co-inhibitory receptors, and CD226 may also transmit co-stimulatory signals.[22–24]

Here, we have identified a defect in GCA Mφs that contributes to the patients' tolerance loss and amplifies disease activity in the affected arteries. GCA Mφs retained the inhibitory ligand CD155 in the endoplasmic reticulum (ER), endowing them with strong immunostimulatory capacities. Such dysfunctional APCs shifted T cell differentiation, expanding CD96^{+} T cells within the memory compartment. CD4^{+} CD96^{+} T cells were functionally committed to produce the effector cytokine IL-9, and loss-of-function and gain-of-function experiments identified IL-9 as a tissue-damaging molecule in vascular inflammation.

RESULTS

Immunoinhibitory receptors in autoimmune vasculitis

In GCA, disease-relevant tolerance defects have been mapped to co-stimulatory and co-inhibitory checkpoints,[5,8] suggesting a key role of T cell receptor signaling strength. Professional APCs express low amounts of PD-L1 and provide strong CD80/86-dependent stimulation.[5,8] Most lesional T cells are high expressers for PD-1, but how the peripheral T cell repertoire is affected by dysbalanced APC-T cell interaction is unknown. We designed a panel of 6 immune checkpoint receptors to comprehensively analyze memory CD4^{+} T cell distributions in the peripheral blood of patients with GCA (n = 8) and age-matched controls (n = 8) (Figures 1A and 1B). CD4^{+} T cells were classified as memory populations based on CD45RA and CCR7 expression. CD45RA^{-} CCR7^{+} T cells identified as central memory cells (Tcms) fell into 5 clusters (clusters 1, 2, 3, 5, and 7). CD45RA^{-} CCR7^{-} effector memory T cells (Tems) were composed of three classification clusters (clusters 4, 8, and 9) and CD45RA^{+}CCR7^{-} terminally differentiated effector memory cells (TEMRAs) formed two distinguishable clusters (clusters 6 and 10).

Expression profiles for the 6 immune checkpoint receptors created a total of 10 clusters across the memory T cell landscape (Figures 1A and 1B). The CD4^{+} Tcm compartment contained 2 subsets of CD96-expressing cells (clusters 1 and 2) and 2 subsets characterized by TIGIT expression (clusters 5 and 7). Tems included CD226-expressing cells, and one subset co-expressed LAG3. End-differentiated TEMRAs mainly had high expression of TIM3 and LAG3, combined with subsets of TIGIT^{low}- and TIM3^{low}-expressing cells. In essence, inhibitory checkpoint receptors were differentially distributed among memory CD4^{+} T cells, with each memory subpopulation having one "marker" checkpoint receptors: CD96 and TIGIT on Tcms, CD226 on Tems, and TIM3 and LAG3 on TEMRAs. PD-1 was rather selective and appeared on TIGIT^{hi} Tcms.

Comparative analysis of circulating memory CD4^{+} T cells in patients with GCA and controls yielded separable distributions of the 10 classification clusters (Figures 1C and 1D). Most noticeable differences occurred within the central memory compartment. Compared with controls, patients' CD96^{hi} Tcms expanded from 10.9% to 16.9% and TIGIT^{hi} Tcms declined from 24.5% to 17.4%. In addition, patient-derived

Figure 1. Enrichment of CD96^{hi} CD4^{+} T cells in giant cell arteritis (GCA)

(A–D) Freshly harvested peripheral blood mononuclear cells (PBMCs) from patients with GCA and age-matched healthy individuals were immunophenotyped by multiparametric flow cytometry for the expression of 6 immunoinhibitory receptors. CD4^{+} memory T cell clusters were classified based on CD45RA and CCR7 expression.

(A) Uniform manifold approximation and projection (UMAP) clustering of memory CD4^{+} T cells, delineating 10 clusters among central memory cells (CD45RA^{-} CCR7^{+}), effector memory cells (CD45RA^{-} CCR7^{-}), and terminally differentiated effector memory cells (TEMRAs; CD45RA^{+} CCR7^{-}). Data are a mix of samples from 8 patients and 8 controls. Plot of 10 identified PhenoGraph clusters is overlaid on the UMAP projection.

(B) Heatmap demonstrating expression of the 6 checkpoint receptors in the 10 clusters based on mean fluorescence intensity (MFI). z scores are shown.

(C–E) UMAP clustering of memory CD4^{+} T cells from 8 healthy individuals (C) and 8 patients with GCA (D). Quantified frequencies (%) of each cluster are presented as pie charts. T cell subsets that are enriched or reduced in patients with GCA are indicated (E).

(F) CD96 mRNA transcripts were quantified by RT-PCR. Data from 10 patients and 10 controls.

(G) CD96 expression quantified by flow cytometry in PBMCs from a confirmation cohort of 16 patients and 16 age-matched controls. MFIs are shown, and each dot represents one patient or control.

(H) CD4^{+} T cells isolated from controls and patients with GCA were stimulated for 0, 3, or 6 days. Kinetics of CD96 expression measured by flow cytometry (n = 4 patients, n = 4 controls).

(I and J) Temporal arteries were collected from diagnostic biopsies of patients with GCA and sinus biopsies from patients with granulomatosis with polyangiitis (GPA).

(I) Targeted tissue transcriptomic analysis of GCA-affected temporal arteries compared with non-inflamed arteries. *CD96* transcripts evaluated by RT-PCR. Each lane represents one tissue sample.

(J) Temporal artery (left) and sinal tissue (right) sections were stained for CD3 (red) and CD96 (green). Nuclei marked by DAPI. Representative images from 4 patients. Frequencies of CD3^{+} CD96^{high} T cells quantified in 50 randomly selected high-power fields. Scale bar: 20 μm. Mean ± SEM with individual values shown.

(F) Mann-Whitney test. (G) Two-tailed unpaired t test. (H) Mann-Whitney test and two-tailed unpaired t test. *p < 0.05, **p < 0.01.

$CD4^+$ memory T cells had a higher frequency of the small $CD226^{hi}$ $LAG3^{hi}$ subset and had a higher proportion of $TIM3^{hi}$ $LAG3^{hi}$ end-differentiated cells (Figure 1E), commonly considered representing exhausted T cells.

We sought to validate the observation that CD96-expressing Tcms were expanded in GCA (Figures 1F, 1G, and S1). GCA $CD4^+$ T cells had higher gene expression (n = 10 controls, n = 10 patients; Figure 1F) and higher CD96 protein expression (n = 16 controls, n = 16 patients; Figures 1G and S1). Kinetic studies confirmed that resting and activated GCA $CD4^+$ T cells expressed higher CD96 cell surface density (Figure 1H).

To assess the disease relevance of $CD4^+CD96^+$ T cells, we analyzed the vasculitic lesions. CD96 mRNA transcripts were abundantly expressed in GCA-affected temporal artery biopsies and were low in non-inflamed arteries (Figure 1I). Multicolor immunofluorescence staining of tissue sections yielded similar results. 90%–95% of the $CD3^+$ T cells in the vasculitic lesions stained positive for CD96 (Figure 1J). Tissues from patients with granulomatosis with polyangiitis (GPA), a small vessel vasculitis affecting sinuses, lungs, and kidneys, contained only a small subset of 5%–10% of $CD96^+$ T cells (Figure 1J).

Together, these data detected a shift of checkpoint receptor-expressing T cells in patients with GCA, localized the shift to the central memory population, and identified the checkpoint receptor CD96 on almost all vasculitic T cells.

CD96 functions as an inhibitory checkpoint receptor in vasculitis

CD96, together with TIGIT and CD226, forms a family of immunoglobulin (Ig) superfamily receptors that interact with nectin and nectin-like molecules.[25] TIGIT is an inhibitory receptor on both T cells and NK cells, and CD226 is believed to also provide activating signals. The intracellular domain of human CD96 contains an immunoreceptor tyrosine-based inhibition motif (ITIM), which confers inhibitory potential. Since the GCA tissue lesions were populated by $CD96^+$ T cells, we aimed at defining the functional role of the receptor in the disease process.

We induced vasculitis in chimeric mice that were engrafted with human arteries and immunoreconstituted with T cells, B cells, and APCs from patients with GCA.[26] To test the functional impact of CD96 signaling, $CD4^+$ T cells were transfected with control or CD96-specific small interfering RNA (siRNA) prior to the adoptive transfer. siRNA transfection reduced CD96 expression by 60% (Figure S2). Low CD96 expression on $CD4^+$ T cells had profound implications for vasculitogenic immunity. Comparison of disease severity in arteries from mice reconstituted with $CD96^{low}$ T cells versus controls demonstrated exacerbation of vasculitis by several readout parameters (Figure 2): density of the mononuclear cell infiltrate, T cell accumulation in the lesion, and enhanced microangiogenesis. The density of tissue-supplying microvessels was assessed by staining for von Willebrand factor $(vWF)^+$ α smooth muscle actin $(\alpha SMA)^+$ lumina (Figure 2E). Adoptive transfer of $CD96^{low}CD4^+$ T cells increased microvessel density by about half (Figure 2F). Also, targeted transcriptomics revealed significantly higher abundance of T cell receptor (TCR) and pro-inflammatory cytokines. Specifically, quantitative comparison in tissues from $CD4^+CD96^{hi}$- versus $CD4^+CD96^{low}$-reconstituted chimeras demonstrated a major impact on T cell effector cytokine production (IFN-γ, IL-21) and innate immunity (tumor necrosis factor [TNF], IL-6, and IL-1β) (Figure 2G).

These loss-of-function experiments established that $CD96^+$ T cells promote vasculitis through T cell- and Mφ-dependent responses and that CD96 is an inhibitory checkpoint receptor in this autoimmune disease.

$CD155^{low}$-expressing APCs in GCA

The identification of CD96 as an immunoinhibitory molecule on vasculitic T cells and the accumulation of $CD96^+$ T cells within the inflamed vessel wall raised the question of whether CD96-dependent signaling is defective and directed attention to the ligand. CD96 interacts with CD155, a receptor expressed on Mφs and dendritic cells[27] markedly upregulated upon activation.[28,29] The CD155 intracellular domain contains an ITIM, classifying the molecule as an immunoinhibitory ligand.

We profiled CD155 expression on monocyte-derived Mφs (MDMs) from patients with GCA, patients with GPA, and age-matched controls (Figures 3A and 3B). In healthy individuals and in patients with GPA, all Mφs expressed high surface density of CD155. In contrast, the entire population of GCA Mφs had low CD155 surface expression, reaching about 50% of the mean fluorescence intensity (MFI) in controls.

To rule out that the $CD155^{low}$ phenotype was a consequence of immunosuppressive therapy, we compared CD155 surface density in untreated and treated patients with GCA (Figure 3C). CD155 expression was unaffected by therapy and was indistinguishably low in both patient cohorts (Figure 3C).

To define the status of CD155 expression in the vasculitic lesions, tissue sections from inflamed temporal arteries were analyzed by dual-color immunofluorescence staining (Figure 3D). Vasculitic lesions were densely populated by $CD68^+$ Mφs, but these tissue-dwelling Mφs had a low signal for CD155 or were entirely negative. Tissue sections from GPA sinusitis served as controls. Again, vasculitic infiltrates were densely populated by $CD68^+$ Mφs, but they displayed a strong signal for CD155, resembling the findings in activated Mφs (Figures 3A–3C).

To begin to understand mechanisms underlying the $CD155^{low}$ phenotype in GCA Mφs, we quantified *CD155* mRNA and CD155 protein in patient-derived and healthy Mφs by RT-PCR and immunoblotting (Figures 3E and 3F). Unexpectedly, GCA and control Mφs produced similar amounts of CD155 transcripts and contained similar concentrations of CD155 protein.

Together, these data assigned the breakdown of CD96-dependent signaling to the APCs, which failed to bring the CD96 ligand CD155 to their surface.

CD155 is trapped in the ER of GCA Mφs

Like other transmembrane proteins, CD155 is produced in the membrane of the ER to traffic to the ER-Golgi intermediate compartment (ERGIC) and the Golgi body.[30] Dependent on how the protein reaches the plasma membrane and whether it is secreted or recycled, it may also associate with endosomes and multivesicular bodies (MVBs).[31–33] To localize the CD155 protein in the cell, we applied a screening process relying on the marking of subcellular organelles. GCA MDMs were stimulated with lipopolysaccharide (LPS) and co-stained for CD155 and a series of organelle markers: calnexin for the ER; P58 for the ERGIC;

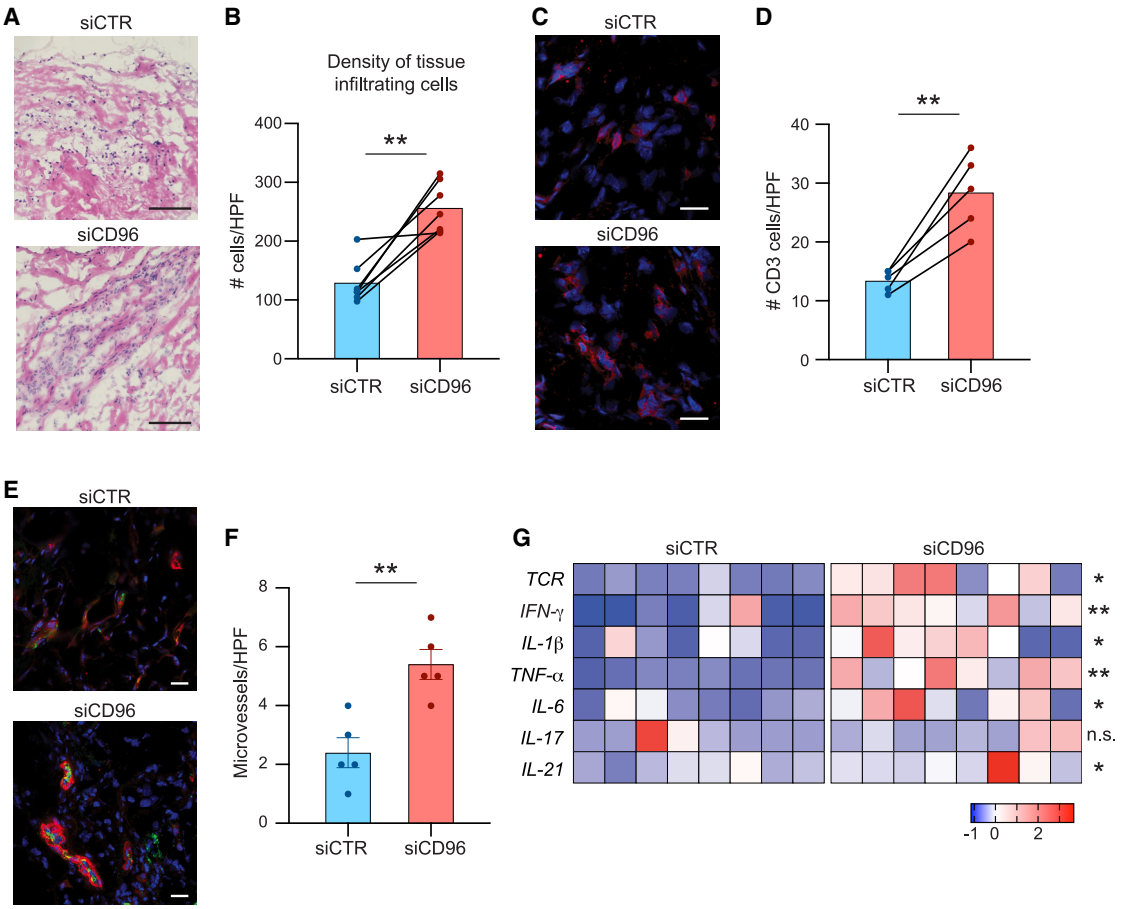

Figure 2. CD96 provides a negative signal in autoimmune vasculitis

CD4$^+$ T cells from patients with GCA were transfected with CD96-specific or control siRNA and adoptively transferred into chimeric NSG mice that had been engrafted with human arteries. Human artery grafts were explanted after 2 weeks and processed for RNA extraction and immunohistochemical analysis.

(A) Tissue sections of explanted arteries were stained with hematoxylin and eosin to assess the invasion of the arterial media by inflammatory cells.

(B) Density of the infiltration was quantified based on nuclear counts in H&E-stained images (n = 7).

(C and D) Tissues were stained for CD3 (red) to estimate the density of tissue infiltrating T cells. Cell numbers were enumerated.

(E and F) Immunostaining of microvessels in the arterial wall. Vascular lumina visualized as vWF$^+$/αSMA$^+$ structures. Enumeration of microvessels shown as bar graphs.

(G) Tissue transcriptomics for T cell receptor (TCR) and cytokines in grafts from mice injected with control or CD96 siRNA-transfected CD4$^+$ T cells. RT-PCR data shown as heatmap.

Scale bars: 100 μm (A) and 20 μm (C and E). Mean ± SEM with individual values shown. (B and D) Two-tailed paired t test. (F) Two-tailed unpaired t test. (G) Two-tailed paired t test or Wilcoxon matched-pairs signed-rank test. *p < 0.05, **p < 0.01, n.s., not significant.

GM130 for the Golgi body; EE1 for the early endosome; CD63 for the late endosome; LC3 for the autophagosome; LAMP2a for the lysosome; and HSP60 for the mitochondria (Figure 4A). We utilized image analysis to estimate co-localization of CD155 with intracellular structures (Figure 4B). Systematic analysis yielded the highest co-localization coefficient with the ER, suggesting that CD155 protein remained at the ER membrane. The signal at the ERGIC was higher than at any of the other organelles, indicating that some of the protein trafficked toward the Golgi and got arrested at the ERGIC. To confirm CD155 retention of CD155 at the ER, we applied immunoblotting of purified ER (Figure 4C). Calnexin served as a control for ER membranes. ER membranes isolated from GCA cells retained about 50% higher amounts of CD155 protein (Figure 4C). CD155-ER co-localization was characteristic for patient Mφs. Direct comparison between healthy and GCA MDMs showed minimal retention of CD155 together with the calnexin signal in controls (Figure S4B).

Protein synthesis at the ER is majorly affected by the activity status of the organelle related to protein folding and lipid synthesis.[34] To evaluate the stress status of the ER in GCA Mφs, we quantified transcripts for 6 genes typically upregulated during the unfolded protein response (UPR) (Figure 4D).[35,36] ER stress assessed in control and patient-derived Mφs by transcript quantification of *ATF4*, *ATF6*, *BiP*, *CHOP*, *TRIB3*, and *XBP*. GCA Mφs showed increased transcription of genes encoding ER chaperones and enzymes involved in ER protein degradation, confirming a state of chronic ER stress. Western blotting for BiP in stimulated Mφs from controls and patients showed a 5-fold upregulation of the ER stress marker in GCA (Figure 4E). To verify that increased ER stress was a relevant mechanism in the tissue infiltrates, we

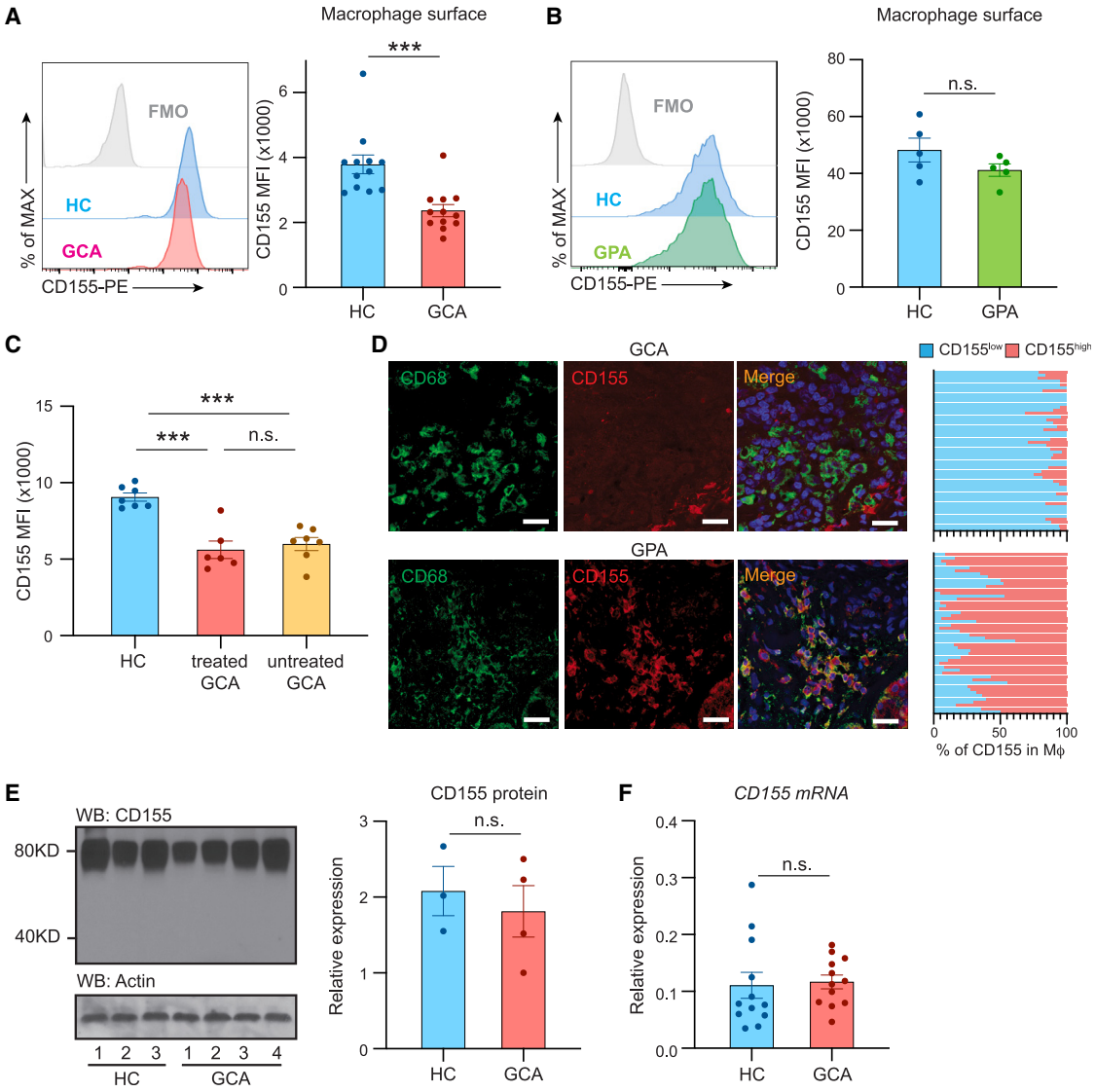

Figure 3. CD155^{low}-expressing antigen-presenting cells in GCA

CD14^{+} cells isolated from the peripheral blood of patients with GCA and age-matched controls were differentiated into monocyte-derived Mφs and stimulated with LPS/IFN-γ.

(A and B) Flow cytometric analysis of CD155 on Mφs from a patient with GCA (A; n = 12) or GPA as a disease control (B; n = 5). Representative histograms and MFI are shown.

(C) Comparison of CD155 expression on Mφs from 7 untreated patients with GCA, 6 corticosteroid-treated patients with GCA, and 7 age-matched controls. Individual MFIs are shown.

(D) Dual-color immunofluorescence staining of tissue sections for CD68 (green) and the checkpoint ligand CD155 (red). Nuclei marked with DAPI (blue). Temporal arteries were collected from patients with GCA and sinonasal biopsies from patients with GPA. Frequencies of CD68^{+} CD155^{high} Mφs were counted in 50 distinct tissue regions. Representative data from 5 tissues. Scale bar: 20 μm.

(E) Immunoblotting of total cell CD155 protein in control and GCA Mφs. β-Actin served as loading control. Bar graph shows protein quantification in individual patients and controls.

(F) Monocyte-derived Mφs were induced from patients with GCA and age-matched controls, and CD155 mRNA transcripts were quantified by RT-PCR. Data from 12 patients and 12 controls.

Mean ± SEM with individual values shown. (A, B, and E) Two-tailed unpaired t test. (C) One-way ANOVA with Tukey's multiple-comparisons test. (F) Mann-Whitney test. ***p < 0.001, n.s., not significant.

stained tissue sections from inflamed temporal arteries for the ER-stress protein BiP (Figure 4F). Tissue lesions from GPA sinusitis served as disease control. The vast majority of CD163^{+} Mφs in the GCA arteries had a strong signal for BiP. In the control tissues, showing granulomatous infiltrates in GPA sinusitis, a strong BiP signal was exclusively seen in CD163^{-}, non-Mφ cells.

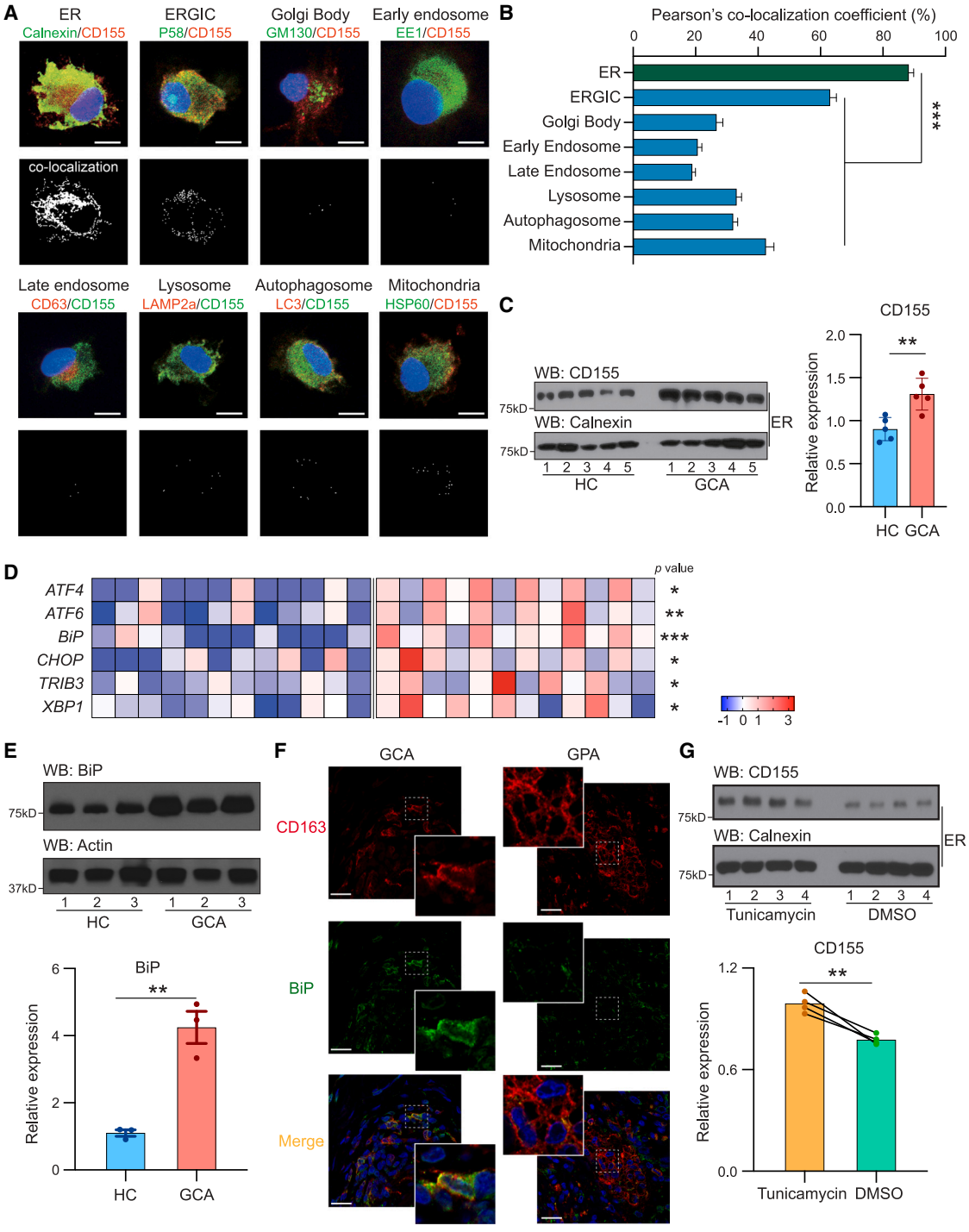

Figure 4. CD155 is trapped in the ER of GCA Mφs

Mφs were induced from peripheral blood precursor cells as in Figure 3.

(A) Dual-color immunofluorescence imaging of Mφs stained for CD155 and cellular organelles. Markers represent the following organelles: ER, calnexin; ERGIC, P58; Golgi body, GM130; early endosome, EE1; late endosome, CD63; lysosome, LAMP2a; autophagosome, LC3; mitochondria, HSP60. Cellular stains were analyzed by imaging software to reveal co-localization as white dots (bottom panel).

(B) Co-localization coefficient between CD155 and individual cell organelles in GCA Mφs. At least 25 cells were quantified from each independent experiment.

(C) The ER fraction was isolated from healthy and GCA Mφs and CD155 protein expression analyzed by immunoblotting. Calnexin served as control. Western blot and quantitative data are shown.

(D) ER stress signatures compared in control and patient-derived Mφs. Transcript levels of ER stress markers were quantified by RT-PCR. z scores are shown (n = 12).

(legend continued on next page)

To test whether the UPR is sufficient to prevent CD155 from leaving the ER and traveling to the Golgi body, we induced ER stress with tunicamycin in healthy Mφs (Figure 4G). ER-bound CD155 protein concentrations were significantly higher in tunicamycin-stressed versus control cells.

From these data, we conclude that Mφ in patients with GCA are in a state of chronic ER stress, inducing the retention of the transmembrane protein CD155 on the ER surface and disabling inhibitory signals directed at T cells.

CD155^{low} Mφs induce IL-9-producing effector T cells

To define pathways through which CD155^{low} Mφs shift T cell differentiation and promote vasculitogenic immunity, we explored the functional impact of CD155^{low} APCs. We stimulated healthy CD4$^+$ T cells with healthy or GCA Mφs and evaluated the induction of effector functions. To avoid a bias introduced by alloantigen recognition, we loaded Mφs with anti-CD3 antibodies to provide consistent TCR triggering. Healthy CD4$^+$ T cells were co-cultured with the two types of Mφs, and the impact on T cell differentiation was monitored by quantifying transcripts for 15 effector cytokines, including all currently known T cell effector cytokines. Effector cytokines were barely detectable in Mφ-free cultures. Compared with controls, GCA Mφs induced a distinct pattern of T cell effector molecules (Figure 5A). Specifically, patient-derived Mφs biased CD4$^+$ T cells toward the production of IL-9, IFN-γ, and IL-21. Notably, several of the effector cytokines, including granulocyte macrophage colony-stimulating factor (GM-CSF), IL-2, IL-17, IL-22, and TNF were unaffected by the origin of the APC (Figure 5A). Also, cytokines associated with Th2-ness (IL-4, IL-5) were equally abundant in T cells activated with control or GCA Mφs.

To verify the differences, we applied flow cytometry staining for intracellular cytokines (Figures 5B–5E). Stimulation by GCA Mφs doubled the frequencies of IL-9-producing CD4$^+$ T cells (Figure 5B), while Mφs from patients with GPA resembled healthy controls (Figure 5C). Similarly, GCA Mφs promoted expansion of IFNγ$^+$ T cells (Th1 cells) (Figure 5D). TNF$^+$ CD4$^+$ T cells appeared with equal frequency when stimulated with healthy or GCA Mφs (Figure 5E).

To explore whether the shift in T cell differentiation, specifically the induction of IL-9-producing T cells, was dependent on CD155 and the interaction of CD155 with CD96, we relied on antibody-blocking studies (Figures 5F–5G). Healthy CD4$^+$ T cells were activated with healthy Mφs in the absence and presence of anti-CD155 antibodies. Frequencies of IL-9-producing CD4$^+$ T cells tripled when the checkpoint was blocked (Figure 5F). Similarly, blocking access to the CD96 receptor resulted in doubling of Th9-comitted effector T cells (Figure 5G).

To summarize, CD155^{low} Mφs from patients with GCA shape the process of T cell differentiation. Lack of CD155-dependent signaling enables the expansion of uncommon, IL-9-producing effector T cells.

IL-9-producing T cells in the vasculitic lesions

To investigate the relevance of Th9 cells in vasculitis, we examined temporal artery biopsies from patients with GCA. Targeted transcriptomics confirmed the presence of IL-9 transcripts exclusively in GCA-affected tissues, with non-inflamed arteries and the non-inflamed aortic wall essentially negative (Figure 6A). Dual-color immunohistochemistry for CD3$^+$ T cells and the IL-9 protein showed clusters of IL-9-producing cells (Figure 6B) in all GCA-affected arteries. These clusters were typically localized outside of the lamina elastic externa. The clustering of the IL-9-producing T cells was suggestive of *in situ* clonal expansion.

To provide quantitative data, we enumerated IL-9$^+$ T cells in the lesions by immunohistochemistry (Figure 6C). Th9 frequencies varied between 6% and 26% of the T cell infiltrate and reached an average of 11.1%. In all GCA arteries, Th9 cells were rare in the intima and media and >90% resided in the adventitia (Figure 6D).

We asked whether IL-9 receptors (IL-9Rs) are expressed in the tissue site to allow the cytokine to interfere with inflammatory and remodeling processes (Figure 6E). Healthy arteries yielded negative to very low signals for IL-9R mRNA. All arteries affected by GCA expressed IL-9R transcripts, displaying similar variability as for IL-9 mRNA itself (Figure 6A).

These data identified IL-9 as one of the effector cytokines of vasculitic T cells and sized the fraction of Th9 cells at about 10%. Th9 cells exclusively mapped to the adventitia, suggesting a role in early steps of vasculitis.

IL-9-producing T cells are pathogenic effector cells

The mere presence of an effector T cell subset in vasculitis lesions does not prove a pathogenic role. We designed loss-of-function and gain-of-function experiments to test the relevance of IL-9 as a driver of autoimmune vasculitis. Arterial wall inflammation was induced in human arteries engrafted into NSG mice. Each chimeric mouse was reconstituted with T cells, B cells, and monocytes donated by a patient with active GCA.

We first explored whether Th9 cells are enriched in the inflamed vessel wall. Frequencies of human CD4$^+$ IL-9$^+$ T cells were measured in the spleen, the blood, and the engrafted artery of chimeric mice. In the spleen and the blood, 5% of CD4$^+$ T cells produced IL-9 (Figure 7A). Frequencies were 3-fold higher in the inflamed arteries, strongly suggestive for selective recruitment of Th9 cells (Figure 7A).

In subsequent experiments, chimeric mice were treated with recombinant human IL-9 (rhIL-9) or vehicle for 1 week. Histologic evaluation of explanted artery grafts connected surplus IL-9 to aggressive inflammation, characterized by destruction of wall

(E) Quantification of the ER stress-related protein BiP in control and GCA Mφs. Representative immunoblot and results from 3 independent experiments.
(F) Dual-color immunofluorescence staining of tissue sections for the Mφ marker CD163 (red) and the ER stress protein BiP (green). Nuclei marked with DAPI (blue). Temporal arteries were collected from patients with GCA. Sinonasal biopsies from patients with GPA served as disease control.
(G) Mφs were treated with the ER stress-inducer tunicamycin or DMSO. ER fractions were isolated, and CD155 was quantified by immunoblotting. Calnexin served as a control. Representative immunoblot and data from 4 independent experiments.
Mean ± SEM with individual data shown. Scale bars: 5 μm (A) and 20 μm (F). (B–E) Two-tailed unpaired t test. (G) Two-tailed paired t test. *$p < 0.05$, **$p < 0.01$, ***$p < 0.001$.

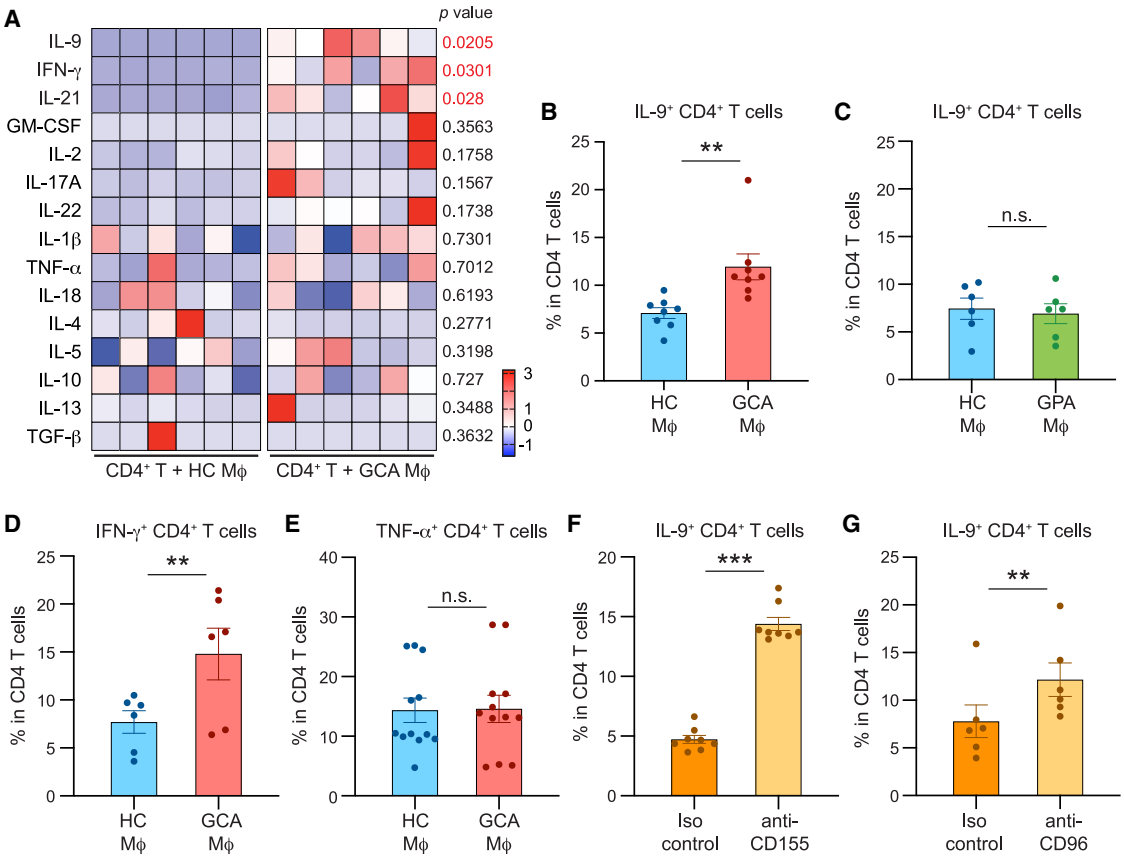

Figure 5. CD155-CD96 interaction promotes differentiation of IL-9-producing effector T cells

Monocyte-derived Mφs were generated from patients with GCA or healthy controls and used as antigen-presenting cells (APCs) for $CD4^+$ T cells. Induction of T cell effector cytokines was assessed by RT-PCR or flow cytometry.

(A) $CD4^+$ T cells from the Mφ-T cell co-cultures were isolated after 72 h. Transcripts for 15 pro-inflammatory effector cytokines were quantified by RT-PCR. Each column represents Mφs from one patient or one control.

(B–E) Frequencies of IL-9-producing (B and C), IFN-γ-producing (D), or TNF-α-producing (E) $CD4^+$ T cells induced by healthy, GCA, or GPA (C) Mφs. Effector cytokines were measured by flow cytometry. Frequencies of cytokine-producing $CD4^+$ T cells from 6 to 12 independent experiments are presented.

(F) $CD4^+$ T cells were stimulated with healthy Mφs in the absence and presence of anti-CD155 antibody. Intracellular IL-9 protein expression in T cells was analyzed by flow cytometry. Frequencies of IL-9-producing $CD4^+$ T cells from 8 experiments.

(G) $CD4^+$ T cells were stimulated with healthy Mφs in the absence and presence of anti-CD96 antibody. Induction of IL-9-producing T cells was determined by flow cytometry. Frequencies of IL-9-producing $CD4^+$ T cells from 6 experiments.

Mean ± SEM with individual values shown. (A and C–G) Two-tailed paired t test. (B) Wilcoxon matched-pairs signed rank test. $^{**}p < 0.01$, $^{***}p < 0.001$, n.s., not significant.

structures, almost complete loss of the medial layer, and moth-eaten areas in the residual media and intima (Figure 7B). The lamina elastica externa and interna were fragmented throughout. Quantification of tissue-infiltrating T cells revealed 3-fold higher numbers of $CD3^+$ T cells in rhIL-9- versus vehicle-treated grafts (Figures 7C and 7D). Comparative analysis of tissue transcriptomes in arteries explanted from vehicle- and rhIL-9-treated chimeras showed that the cytokine was able to induce robust vasculitis (Figure 7E). Transcripts for the T cell cytokines IFN-γ, IL-17, and IL-21 were all upregulated. In parallel, upregulation of *CD80* and *CD86* transcripts provided evidence for Mφ activation, supported by markedly higher *IL-1β*, *IL-6*, and *TNF* mRNA.

To validate the pathogenic role of IL-9 in loss-of-function experiments, we used anti-IL-9 antibody (Ab)-blocking studies. Vasculitis was induced in artery-engrafted NSG mice, and chimeras were treated with anti-IL-9 Ab or isotype-control IgG. Dense inflammatory infiltrates penetrated throughout all wall layers in the control IgG-treated grafts, and anti-IL-9-treated tissues had sparse infiltrates (Figure 7B). The density of the T cell infiltrates declined markedly in anti-IL-9-treated grafts (Figure 7C). Blocking of IL-9 resulted in a sharp reduction of tissue-invading T cells (Figure 7D). Anti-IL-9 Ab reduced the number of tissue-infiltrating T cells from 50 to 20 cells/high-power field (HPF). Tissue transcriptomics for a core module of inflammatory markers are presented as a heatmap and show the profound effect of IL-9 blockade on vascular inflammation (Figure 7F). Selective inhibition of IL-9 resulted in suppression of T cell effector cytokines, including IFN-γ, IL-17, and IL-21. A sharp reduction of IL-1β, IL-6, and TNF in the tissue of anti-IL-9-treated chimeras confirmed the inhibitory effect of Ab treatment on innate immunity. *CD80* and *CD86*

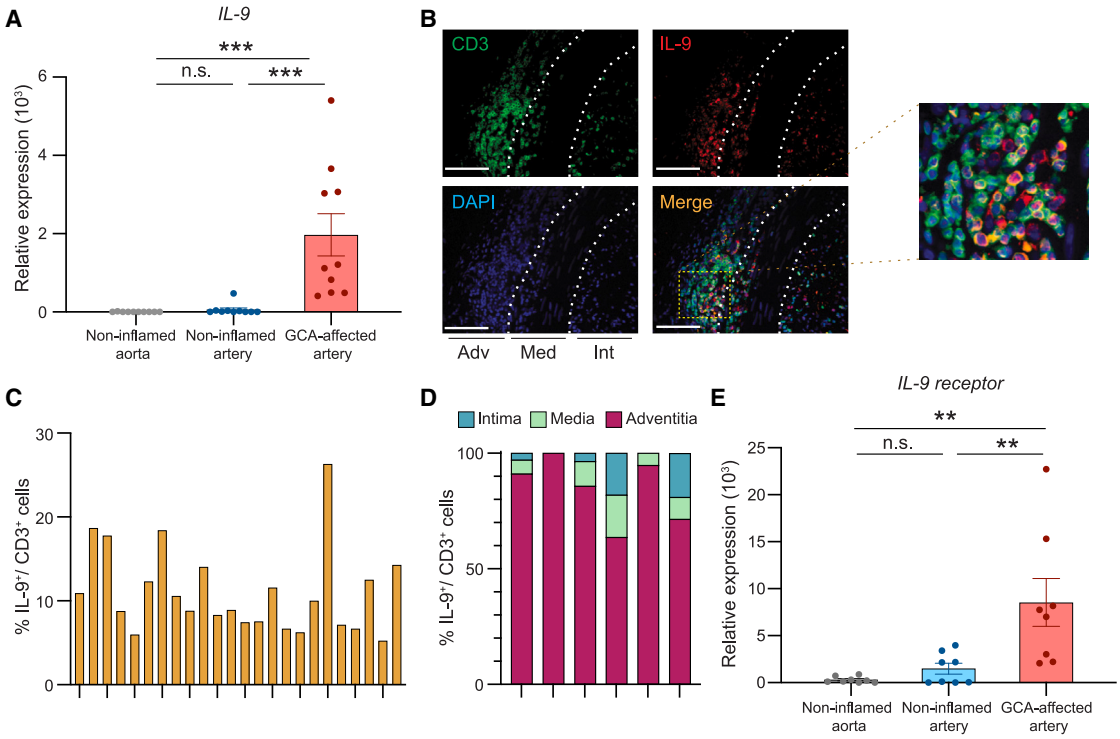

Figure 6. IL-9⁺ T cells in the vasculitic lesions of GCA

Arteries affected with GCA were collected by diagnostic biopsy.

(A) Tissue transcriptomics (RT-PCR) for IL-9 in GCA-affected arteries; normal, non-inflamed arteries; and normal, non-inflamed aorta (n = 10 samples each).

(B–D) Tissue sections from GCA arteries were immunostained with anti-CD3 antibody (green) and anti-IL-9 antibody (red). Nuclei marked with DAPI (blue).

(B) Representative images from 6 arteries. Scale bar: 100 μm.

(C) Frequencies of $CD3^+$ $IL\text{-}9^+$ cells in $CD3^+$ T cells in independent high-power fields.

(D) Distribution of IL-9-producing T cells in the intimal, medial, and adventitial layers. Data from 6 arteries.

(E) IL-9 receptor transcripts expressed in GCA-affected arteries compared with normal, non-inflamed aortas and arteries (RT-PCR) (n = 8 samples each).

Mean ± SEM with individual values shown. (A and E) One-way ANOVA with Tukey's multiple-comparisons test was used. $^{**}p < 0.01$, $^{***}p < 0.001$, n.s., not significant.

transcripts were highly sensitive to anti-IL-9 treatment, confirming IL-9's role in regulating tissue Mφs (Figure 7F).

To provide evidence that the inflammation resulting from a defective CD155-CD96 checkpoint was dependent on IL-9, we induced vasculitis with intact or CD96 siRNA-transfected $CD4^+$ T cells and combined it with anti-IL-9 Ab treatment (Figures 7G–7I). As in Figure 2, CD96 loss of function in the adoptively transferred $CD4^+$ T cells resulted in aggressive vasculitis, with dense wall infiltrates and wide-spread neoangiogenesis (Figures 7G–7H). Blocking IL-9 alleviated the wall infiltrates and reduced intrawall angiogenesis. Tissue transcriptomic analysis confirmed that anti-IL-9 treatment reversed the exacerbation of vasculitis by blunting the induction of innate and adaptive effector cytokines (Figure 7I).

Together, these data established IL-9 as a driver cytokine of vascular inflammation, endowed with regulatory control over innate and adaptive immune responses in the inflamed arteries.

DISCUSSION

Immune checkpoints control the initiation, the duration, the strength, and the outcome of immune responses, and checkpoint blockade leads to tissue inflammation mimicking autoimmune disease. Current work implicates a defective CD155-CD96 checkpoint in spontaneous autoimmunity manifesting as large vessel vasculitis. Patients with GCA had a shift in their functional T cell repertoire, expanding $CD96^+$ memory CD4 T cells in the blood and in the inflamed arteries. Knockdown experiments assigned the CD96 receptor to an inhibitory pathway, defining vasculitis as the consequence of insufficient CD96 signaling. APCs from patients with vasculitis, including Mφs in the vasculitic lesions, were typically low in the expression of CD155, the ligand interacting with CD96. $CD155^{lo}$ Mφs produced the protein but retained it on the ER membranes. $CD155^{lo}$ Mφs induced a program of T cell differentiation that favored the IL-9-producing lineage. Loss-of-function and gain-of-function experiments confirmed that IL-9 is a key driver of vasculitis, promoting vascular remodeling and tissue-destructive immunity. These data link the CD155-CD96 checkpoint to the differentiation and the expansion of the Th9 lineage and classify GCA as a disease of checkpoint failure that is caused by abnormal intracellular trafficking of the checkpoint ligand CD155.

IL-9 has a pleiotropic range of functions, has been associated with allergic disease and anti-parasitic immune responses,[37,38] and aggravates the development of atherosclerosis.[39] A variety of cell types can produce IL-9, including mast cells, NKT cells,

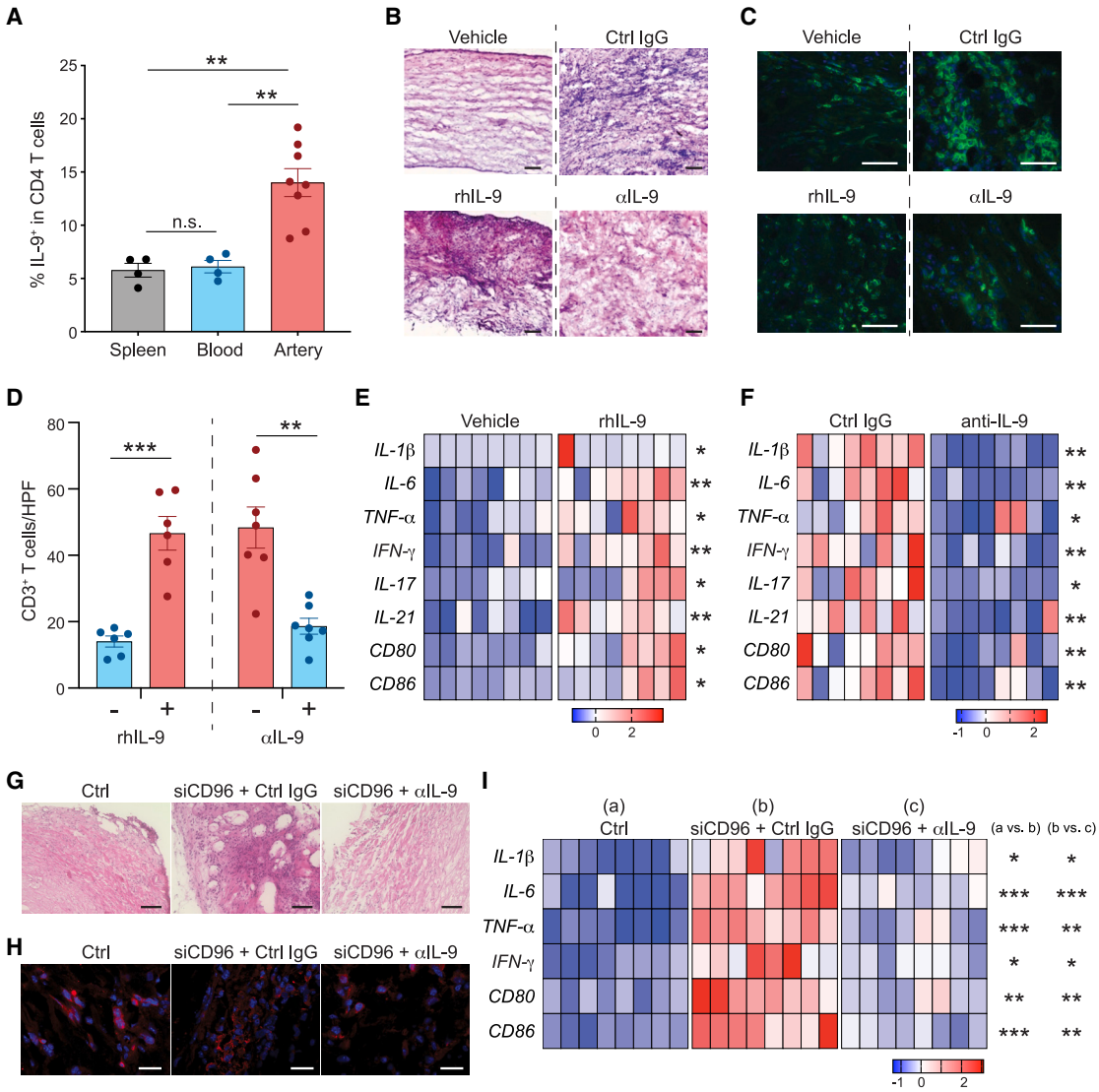

Figure 7. IL-9 promotes tissue damage in autoimmune vasculitis

Immunodeficient NSG mice were engrafted with human arteries and immunoreconstituted with PBMCs from a patient with active GCA.

(A) Human CD4$^+$ T cells were extracted from the mouse spleen, the murine blood, and the explanted artery grafts. Frequencies of IL-9-producing T cells were determined by fluorescence-activated cell sorting (FACS) utilizing intracellular staining.

(B–F) Chimeric mice carrying the same artery and the same PBMC were assigned to one of four treatment arms and were treated for 1 week by intraperitoneal injection on alternative days: vehicle, rhIL-9 (200 ng), control IgG (100 μg/intraperitoneal injection), or anti-IL-9 antibody (100 μg/intraperitoneal injection).

(B) Tissue sections of explanted arteries were stained with H&E. Representative images from one of 8 artery grafts.

(C) PBS- or rhIL-9-treated arteries (n = 6 each) or control or anti-IL-9 treated arteries (n = 7 each) were immunostained with anti-CD3 antibody (green) and DAPI (blue). Representative immunostains are presented.

(D) The density of the T cell infiltrate in arteries form the 4 treatment arms was determined by enumerating CD3$^+$ T cell in tissue sections. Each dot represents one artery.

(E) Gene expression profiling of inflammatory genes in extracts from the explanted arteries. RT-PCR analysis of 8 arteries treated with either vehicle or rhIL-9 shown as heatmap in z scores.

(F) Gene expression profiling for inflammatory cytokines and co-stimulatory ligands in tissue extracts of control- and anti-IL-9-treated blood vessels by RT-PCR.

(G–I) CD4$^+$ T cells from patients with GCA were transfected with CD96-specific or control siRNA and adoptively transferred into artery-engrafted NSG mice as in Figure 2. Chimeras were assigned to two treatment arms: injection of anti-IL-9 antibody or control IgG as in (B)–(F).

(G) Tissue sections of explanted arteries were stained with H&E. Representative images from one of 8 artery grafts.

(H) Tissue sections were stained for CD3 (red) to mark tissue infiltrating T cells and compare the density of tissue infiltrates.

(I) Gene expression profiling for inflammatory cytokines and co-stimulatory ligands in tissue extracts of control-, siCD96-, and siCD96 plus anti-IL-9-treated blood vessels by RT-PCR.

Mean ± SEM with individual values shown. Scale bars: 100 μm (B and G) and 20 μm (C and H). (A and I) One-way ANOVA with Tukey's multiple-comparisons test. (D– F) Two tailed paired t test. *p < 0.05, **p < 0.01, ***p < 0.001, n.s., not significant.

Th2 cells, Th17 cells, regulatory T cells (Tregs), and group two innate lymphoid cells (ILC2s), but by far the most important source is CD4$^+$ T cells committed to the Th9 lineage.[40–45] Th9 differentiation requires a complex transcription factor network, including STAT6, IRF4, the transcription factor PU.1, and the basic leucine zipper transcription factor, ATF-like (BATF),[46] classifying Th9 cells as a distinct and homogeneous lineage. IL-9 has anti-tumor activity,[47–49] in line with its tissue-destructive capabilities. High expression of IL-9 mRNA in inflammatory bowel disease (IBD) has identified Th9 cells as disease drivers in ulcerative colitis.[50,51] However, dependent on timing and context of inflammatory conditions *in vivo*, IL-9 may be anti-inflammatory.[52] The abundance of IL-9 and IL-9Rs in GCA-affected arteries identifies IL-9 as an inflammatory amplifier in vasculitis. IL-9Rs were broadly expressed in vascular and infiltrating cells. The degree of tissue destruction in arteries exposed to excess IL-9 was unexpected. Usually, inflammatory attack to the vessel wall elicits neoangiogenesis and intimal hyperplasia,[18] compatible with a maladaptive tissue healing response. Arteries from IL-9-treated chimeras had essentially lost the medial layer; elastic membranes were fragmented, and the tissue had areas of complete destruction. Th9 cells accounted for about 10% of the T cell infiltrate in vasculitic arteries, raising the question of how this relatively small effector subset can determine disease intensity. Th9 cells sat almost exclusively in the adventitia, arranged in dense T cell clusters, where they may have access to adventitial dendritic cells that control tissue tolerance.[53]

In current work, IL-9 derived mainly from CD96$^+$ T cells, confirming studies in IBD that have associated low CD96 signal strength with high IL-9 production.[54] CD96 is expressed on CD4$^+$ T cells, CD8$^+$ T cells, and NK cells and, together with CD226 and TIGIT, is known to bind to nectins and nectin-like proteins.[22] Members of the CD96/TIGIT/CD226 receptor family provide co-stimulatory and co-inhibitory signals. CD226 enhances T cell activation, TIGIT is an established co-inhibitory receptor.[23,55–57] CD96 appears to transmit both positive as well as negative signals,[58,59] but in the setting of large vessel vasculitis, loss of CD96 signaling profoundly exacerbated disease. These data are in line with previous reports in which CD96$^+$ Th9 cells displayed strong pro-inflammatory capacities.[54] The tissue-destructive pattern of CD96$^+$ T cells in vasculitis mimicked the profound inflammatory potential of such cells in the murine colon, producing aggressive colitis. Tissue-damaging effector functions were clearly linked to IL-9 release, as documented by Ab-blocking studies and the tissue destruction mediated by recombinant IL-9.

Data support the concept that CD96$^+$ Th9 cells become pathogenic effectors due to insufficient suppression. The peripheral blood and the inflamed tissue of patients with GCA contained expanded numbers of CD4$^+$ CD96$^+$ T cells. In the immunophenotypic studies, CD96 was predominantly expressed on human memory CD4$^+$ T cells, with a small population of effector memory cells positive for the receptor. Remarkably, TIGIT could be placed on a distinct population of memory CD4$^+$ T cells, and PD-1 was co-expressed with TIGIT in a subset of memory cells. Like CD96, TIGIT was absent from most Tems, but unlike CD96, TIGIT was detected on a subpopulation of end-differentiated CD4 T cells (Figure 1). Vasculitis-associated shifts in the functional T cell repertoire included the enrichment of CD96$^+$ CD4$^+$ T cells and the decline of TIGIT$^+$ CD4$^+$ T cells, clearly indicating independent regulation of these memory T cell populations despite their shared ability to interact with CD155. The cytoplasmic tails of CD96 and TIGIT both contain an immunoreceptor tyrosine-based inhibition motif (ITIM) but possibly access differential signaling pathways to direct differentiating T cells toward expansion or contraction.

The pinnacle defect that disabled the CD155-CD96 pathway in GCA related to the processing of CD155. Low surface expression of CD155 prevented APCs from patients with GCA from delivering a CD96-dependent stop signal. Surprisingly, the total cell amount of CD155 was well maintained in such CD155^{low} APCs, and mRNA concentrations for the CD155-encoding gene *PVR* were indistinguishable in patients and controls. CD155 was produced but retained in the cytosol, specifically in the ER. ER retention of CD155 was associated with an ER stress response and was inducible with the ER stressor tunicamycin. Signals leading to excess ER stress in GCA Mφs are currently unknown, and the precise molecular mechanisms leading to ER retention require further investigation. Several mechanisms of posttranslational processing of CD155 have been described. A recent study connected excess expression and excess inhibitory function of CD155 to alterations in *PVR* mRNA methylation and stability,[20] creating CD155^{hi} inhibitory Mφs in patients with coronary artery disease. As a receptor for poliovirus, the protein has complex subcellular trafficking pathways, partially regulated by posttranslational modifications such as SUMOylation and partially by interacting with the dynein light chain Tctex-1, which transports the protein to distinct subcellular localizations.[60,61]

The study has important clinical implications and can help pave the way for checkpoint-directed therapy in spontaneous autoimmune disease. In GCA, the CD155-CD96 checkpoint is the second checkpoint of pathogenic relevance, coming in after the PD-L1-PD1 checkpoint.[5] For both of these checkpoints, *in vivo* data have documented that their failing enhanced disease activity. Molecular mechanisms underlying the deficiency of PD-L1/PD-1 signaling in GCA are not understood, but current data have identified a processing defect in the checkpoint ligand CD155 as a steppingstone to autoimmunity. Notably, the loss in negative signals provided by APCs had profound impact on the fate decisions of T cells, guiding them toward the Th9 lineage. CD96 is expressed relatively late in the T cell activation program, predictably affecting contraction of the T cell response more than the induction. This disease mechanism in autoimmune disease provides opportunities for repair, which could begin with restoring CD155 intracellular trafficking but could also extend to blocking the expansion of IL-9-producing, tissue-invasive T cells and their effector cytokines.

Limitations of the study

The current study links hypoactivity of the CD155-CD96 immune checkpoint to GCA, adding a second faulty immune checkpoint to the pathology of this vasculitis. The question arises whether GCA is a syndrome of "lost inhibition," with multiple flawed immune checkpoints. We did not solve the molecular mechanism causing ER retention of CD155, which may be relevant for an array of inhibitory ligands and could ultimately identify GCA as

a syndrome of ER pathology. Finally, we did not clarify how IL-9 causes vascular destruction, how IL-9 communicates with immune and stromal cells in the vessel wall, and whether IL-9 represents a clinically relevant biomarker of vasculitis.

STAR★METHODS

Detailed methods are provided in the online version of this paper and include the following:

- KEY RESOURCES TABLE
- RESOURCE AVAILABLITY
  - Lead contact
  - Materials availability
  - Data and code availability
- EXPERIMENTAL MODEL AND SUBJECT DETAILS
  - Patients and tissues
  - Cell preparation and culture
  - Human artery-severe combined immunodeficiency mouse chimeras
- METHOD DETAILS
  - Macrophage-T cell co-cultures
  - Quantitative reverse transcription polymerase chain reaction (RT-PCR)
  - Flow cytometry and multiparametric phenotyping
  - Immunohistochemistry and immunofluorescence
- QUANTIFICATION AND STATISTICAL ANALYSIS

SUPPLEMENTAL INFORMATION

Supplemental information can be found online at https://doi.org/10.1016/j.xcrm.2023.101012.

ACKNOWLEDGMENTS

This work was supported by the National Institutes of Health (R01AR042527, R01AI108906, R01HL142068, and R01HL117913 to C.M.W. and R01AI108891, R01AG045779, U19AI057266, and R01AI129191 to J.J.G.).

AUTHOR CONTRIBUTIONS

Conceptualization, C.M.W., J.J.G., and S.O.; formal analysis, S.O. and C.W.; investigation, S.O., C.W., R.W., H.Z., M.A., and G.J.B.; patient recruitment, C.M.W., J.J.G., S.O., G.J.B., M.C.B., J.J.M., and K.J.W.; writing – original draft, C.M.W., J.J.G., and S.O.; supervision, C.M.W., J.J.G., and G.J.B.; funding acquisition, C.M.W. and J.J.G.

DECLARATION OF INTERESTS

K.J.W. has received clinical trial support from Eli Lilly, GSK, and Kiniksa; he received consulting fees and honoraria from Chemocentryx.

Received: October 24, 2022
Revised: February 13, 2023
Accepted: March 21, 2023
Published: April 18, 2023

REFERENCES

1. Baumeister, S.H., Freeman, G.J., Dranoff, G., and Sharpe, A.H. (2016). Co-inhibitory pathways in immunotherapy for cancer. Annu. Rev. Immunol. *34*, 539–573. https://doi.org/10.1146/annurev-immunol-032414-112049.
2. Fritz, J.M., and Lenardo, M.J. (2019). Development of immune checkpoint therapy for cancer. J. Exp. Med. *216*, 1244–1254. https://doi.org/10.1084/jem.20182395.
3. Okazaki, T., and Honjo, T. (2007). PD-1 and PD-1 ligands: from discovery to clinical application. Int. Immunol. *19*, 813–824. https://doi.org/10.1093/intimm/dxm057.
4. Ramos-Casals, M., Brahmer, J.R., Callahan, M.K., Flores-Chávez, A., Keegan, N., Khamashta, M.A., Lambotte, O., Mariette, X., Prat, A., and Suárez-Almazor, M.E. (2020). Immune-related adverse events of checkpoint inhibitors. Nat. Rev. Dis. Prim. *6*, 38. https://doi.org/10.1038/s41572-020-0160-6.
5. Zhang, H., Watanabe, R., Berry, G.J., Vaglio, A., Liao, Y.J., Warrington, K.J., Goronzy, J.J., and Weyand, C.M. (2017). Immunoinhibitory checkpoint deficiency in medium and large vessel vasculitis. Proc. Natl. Acad. Sci. USA *114*, E970–E979. https://doi.org/10.1073/pnas.1616848114.
6. Pugh, D., Karabayas, M., Basu, N., Cid, M.C., Goel, R., Goodyear, C.S., Grayson, P.C., McAdoo, S.P., Mason, J.C., Owen, C., et al. (2022). Large-vessel vasculitis. Nat. Rev. Dis. Prim. *7*, 93. https://doi.org/10.1038/s41572-021-00327-5.
7. Weyand, C.M., and Goronzy, J.J. (2013). Immune mechanisms in medium and large-vessel vasculitis. Nat. Rev. Rheumatol. *9*, 731–740. https://doi.org/10.1038/nrrheum.2013.161.
8. Zhang, H., Watanabe, R., Berry, G.J., Nadler, S.G., Goronzy, J.J., and Weyand, C.M. (2019). CD28 signaling controls metabolic fitness of pathogenic T cells in medium and large vessel vasculitis. J. Am. Coll. Cardiol. *73*, 1811–1823. https://doi.org/10.1016/j.jacc.2019.01.049.
9. Wen, Z., Shen, Y., Berry, G., Shahram, F., Li, Y., Watanabe, R., Liao, Y.J., Goronzy, J.J., and Weyand, C.M. (2017). The microvascular niche instructs T cells in large vessel vasculitis via the VEGF-Jagged1-Notch pathway. Sci. Transl. Med. *9*, eaal3322. https://doi.org/10.1126/scitranslmed.aal3322.
10. Ciccia, F., Rizzo, A., Guggino, G., Cavazza, A., Alessandro, R., Maugeri, R., Cannizzaro, A., Boiardi, L., Iacopino, D.G., Salvarani, C., and Triolo, G. (2015). Difference in the expression of IL-9 and IL-17 correlates with different histological pattern of vascular wall injury in giant cell arteritis. Rheumatology *54*, 1596–1604. https://doi.org/10.1093/rheumatology/kev102.
11. Terrier, B., Geri, G., Chaara, W., Allenbach, Y., Rosenzwajg, M., Costedoat-Chalumeau, N., Fouret, P., Musset, L., Benveniste, O., Six, A., et al. (2012). Interleukin-21 modulates Th1 and Th17 responses in giant cell arteritis. Arthritis Rheum. *64*, 2001–2011. https://doi.org/10.1002/art.34327.
12. Jin, K., Wen, Z., Wu, B., Zhang, H., Qiu, J., Wang, Y., Warrington, K.J., Berry, G.J., Goronzy, J.J., and Weyand, C.M. (2021). NOTCH-induced rerouting of endosomal trafficking disables regulatory T cells in vasculitis. J. Clin. Invest. *131*, e136042. https://doi.org/10.1172/JCI136042.
13. Hunder, G.G., Bloch, D.A., Michel, B.A., Stevens, M.B., Arend, W.P., Calabrese, L.H., Edworthy, S.M., Fauci, A.S., Leavitt, R.Y., Lie, J.T., et al. (1990). The American College of Rheumatology 1990 criteria for the classification of giant cell arteritis. Arthritis Rheum. *33*, 1122–1128. https://doi.org/10.1002/art.1780330810.
14. Maleszewski, J.J., Younge, B.R., Fritzlen, J.T., Hunder, G.G., Goronzy, J.J., Warrington, K.J., and Weyand, C.M. (2017). Clinical and pathological evolution of giant cell arteritis: a prospective study of follow-up temporal artery biopsies in 40 treated patients. Mod. Pathol. *30*, 788–796. https://doi.org/10.1038/modpathol.2017.10.
15. Weyand, C.M., and Goronzy, J.J. (2023). Immunology of giant cell arteritis. Circ. Res. *132*, 238–250. https://doi.org/10.1161/CIRCRESAHA.122.322128.
16. Watanabe, R., Maeda, T., Zhang, H., Berry, G.J., Zeisbrich, M., Brockett, R., Greenstein, A.E., Tian, L., Goronzy, J.J., and Weyand, C.M. (2018). MMP (matrix metalloprotease)-9-producing monocytes enable T cells to invade the vessel wall and cause vasculitis. Circ. Res. *123*, 700–715. https://doi.org/10.1161/CIRCRESAHA.118.313206.

17. Watanabe, R., Hilhorst, M., Zhang, H., Zeisbrich, M., Berry, G.J., Wallis, B.B., Harrison, D.G., Giacomini, J.C., Goronzy, J.J., and Weyand, C.M. (2018). Glucose metabolism controls disease-specific signatures of macrophage effector functions. JCI Insight *3*, e123047. https://doi.org/10.1172/jci.insight.123047.

18. Piggott, K., Biousse, V., Newman, N.J., Goronzy, J.J., and Weyand, C.M. (2009). Vascular damage in giant cell arteritis. Autoimmunity *42*, 596–604. https://doi.org/10.1080/08916930903002495.

19. Shirai, T., Nazarewicz, R.R., Wallis, B.B., Yanes, R.E., Watanabe, R., Hilhorst, M., Tian, L., Harrison, D.G., Giacomini, J.C., Assimes, T.L., et al. (2016). The glycolytic enzyme PKM2 bridges metabolic and inflammatory dysfunction in coronary artery disease. J. Exp. Med. *213*, 337–354. https://doi.org/10.1084/jem.20150900.

20. Zhao, T.V., Hu, Z., Ohtsuki, S., Jin, K., Wu, B., Berry, G.J., Frye, R.L., Goronzy, J.J., and Weyand, C.M. (2022). Hyperactivity of the CD155 immune checkpoint suppresses anti-viral immunity in patients with coronary artery disease. Nat. Cardiovasc. Res. *1*, 634–648. https://doi.org/10.1038/s44161-022-00096-8.

21. Kučan Brlić, P., Lenac Roviš, T., Cinamon, G., Tsukerman, P., Mandelboim, O., and Jonjić, S. (2019). Targeting PVR (CD155) and its receptors in anti-tumor therapy. Cell. Mol. Immunol. *16*, 40–52. https://doi.org/10.1038/s41423-018-0168-y.

22. Georgiev, H., Ravens, I., Papadogianni, G., and Bernhardt, G. (2018). Coming of age: CD96 emerges as modulator of immune responses. Front. Immunol. *9*, 1072. https://doi.org/10.3389/fimmu.2018.01072.

23. Shibuya, A., Campbell, D., Hannum, C., Yssel, H., Franz-Bacon, K., McClanahan, T., Kitamura, T., Nicholl, J., Sutherland, G.R., Lanier, L.L., and Phillips, J.H. (1996). DNAM-1, a novel adhesion molecule involved in the cytolytic function of T lymphocytes. Immunity *4*, 573–581. https://doi.org/10.1016/s1074-7613(00)70060-4.

24. Yu, X., Harden, K., Gonzalez, L.C., Francesco, M., Chiang, E., Irving, B., Tom, I., Ivelja, S., Refino, C.J., Clark, H., et al. (2009). The surface protein TIGIT suppresses T cell activation by promoting the generation of mature immunoregulatory dendritic cells. Nat. Immunol. *10*, 48–57. https://doi.org/10.1038/ni.1674.

25. Chan, C.J., Andrews, D.M., and Smyth, M.J. (2012). Receptors that interact with nectin and nectin-like proteins in the immunosurveillance and immunotherapy of cancer. Curr. Opin. Immunol. *24*, 246–251. https://doi.org/10.1016/j.coi.2012.01.009.

26. Piggott, K., Deng, J., Warrington, K., Younge, B., Kubo, J.T., Desai, M., Goronzy, J.J., and Weyand, C.M. (2011). Blocking the NOTCH pathway inhibits vascular inflammation in large-vessel vasculitis. Circulation *123*, 309–318. https://doi.org/10.1161/CIRCULATIONAHA.110.936203.

27. Lupo, K.B., and Matosevic, S. (2020). CD155 immunoregulation as a target for natural killer cell immunotherapy in glioblastoma. J. Hematol. Oncol. *13*, 76. https://doi.org/10.1186/s13045-020-00913-2.

28. Chan, C.J., Martinet, L., Gilfillan, S., Souza-Fonseca-Guimaraes, F., Chow, M.T., Town, L., Ritchie, D.S., Colonna, M., Andrews, D.M., and Smyth, M.J. (2014). The receptors CD96 and CD226 oppose each other in the regulation of natural killer cell functions. Nat. Immunol. *15*, 431–438. https://doi.org/10.1038/ni.2850.

29. Kamran, N., Takai, Y., Miyoshi, J., Biswas, S.K., Wong, J.S.B., and Gasser, S. (2013). Toll-like receptor ligands induce expression of the costimulatory molecule CD155 on antigen-presenting cells. PLoS One *8*, e54406. https://doi.org/10.1371/journal.pone.0054406.

30. Shikano, S., and Li, M. (2003). Membrane receptor trafficking: evidence of proximal and distal zones conferred by two independent endoplasmic reticulum localization signals. Proc. Natl. Acad. Sci. USA *100*, 5783–5788. https://doi.org/10.1073/pnas.1031748100.

31. Bourne, H.R., Sanders, D.A., and McCormick, F. (1990). The GTPase superfamily: a conserved switch for diverse cell functions. Nature *348*, 125–132. https://doi.org/10.1038/348125a0.

32. Gordon, D.M., Lyver, E.R., Lesuisse, E., Dancis, A., and Pain, D. (2006). GTP in the mitochondrial matrix plays a crucial role in organellar iron homoeostasis. Biochem. J. *400*, 163–168. https://doi.org/10.1042/BJ20060904.

33. Roche, P.A. (1999). Intracellular protein traffic in lymphocytes: "how do I get THERE from HERE"? Immunity *11*, 391–398. https://doi.org/10.1016/s1074-7613(00)80114-4.

34. Hotamisligil, G.S. (2010). Endoplasmic reticulum stress and the inflammatory basis of metabolic disease. Cell *140*, 900–917. https://doi.org/10.1016/j.cell.2010.02.034.

35. Bommiasamy, H., Back, S.H., Fagone, P., Lee, K., Meshinchi, S., Vink, E., Sriburi, R., Frank, M., Jackowski, S., Kaufman, R.J., and Brewer, J.W. (2009). ATF6alpha induces XBP1-independent expansion of the endoplasmic reticulum. J. Cell Sci. *122*, 1626–1636. https://doi.org/10.1242/jcs.045625.

36. Sriburi, R., Jackowski, S., Mori, K., and Brewer, J.W. (2004). XBP1: a link between the unfolded protein response, lipid biosynthesis, and biogenesis of the endoplasmic reticulum. J. Cell Biol. *167*, 35–41. https://doi.org/10.1083/jcb.200406136.

37. Nicolaides, N.C., Holroyd, K.J., Ewart, S.L., Eleff, S.M., Kiser, M.B., Dragwa, C.R., Sullivan, C.D., Grasso, L., Zhang, L.Y., Messler, C.J., et al. (1997). Interleukin 9: a candidate gene for asthma. Proc. Natl. Acad. Sci. USA *94*, 13175–13180. https://doi.org/10.1073/pnas.94.24.13175.

38. Shimbara, A., Christodoulopoulos, P., Soussi-Gounni, A., Olivenstein, R., Nakamura, Y., Levitt, R.C., Nicolaides, N.C., Holroyd, K.J., Tsicopoulos, A., Lafitte, J.J., et al. (2000). IL-9 and its receptor in allergic and nonallergic lung disease: increased expression in asthma. J. Allergy Clin. Immunol. *105*, 108–115. https://doi.org/10.1016/s0091-6749(00)90185-4.

39. Zhang, W., Tang, T., Nie, D., Wen, S., Jia, C., Zhu, Z., Xia, N., Nie, S., Zhou, S., Jiao, J., et al. (2015). IL-9 aggravates the development of atherosclerosis in ApoE-/- mice. Cardiovasc. Res. *106*, 453–464. https://doi.org/10.1093/cvr/cvv110.

40. Elyaman, W., Bradshaw, E.M., Uyttenhove, C., Dardalhon, V., Awasthi, A., Imitola, J., Bettelli, E., Oukka, M., van Snick, J., Renauld, J.C., et al. (2009). IL-9 induces differentiation of TH17 cells and enhances function of FoxP3+ natural regulatory T cells. Proc. Natl. Acad. Sci. USA *106*, 12885–12890. https://doi.org/10.1073/pnas.0812530106.

41. Gounni, A.S., Nutku, E., Koussih, L., Aris, F., Louahed, J., Levitt, R.C., Nicolaides, N.C., and Hamid, Q. (2000). IL-9 expression by human eosinophils: regulation by IL-1beta and TNF-alpha. J. Allergy Clin. Immunol. *106*, 460–466. https://doi.org/10.1067/mai.2000.109172.

42. Hültner, L., Kölsch, S., Stassen, M., Kaspers, U., Kremer, J.P., Mailhammer, R., Moeller, J., Broszeit, H., and Schmitt, E. (2000). In activated mast cells, IL-1 up-regulates the production of several Th2-related cytokines including IL-9. J. Immunol. *164*, 5556–5563. https://doi.org/10.4049/jimmunol.164.11.5556.

43. Lu, L.F., Lind, E.F., Gondek, D.C., Bennett, K.A., Gleeson, M.W., Pino-Lagos, K., Scott, Z.A., Coyle, A.J., Reed, J.L., Van Snick, J., et al. (2006). Mast cells are essential intermediaries in regulatory T-cell tolerance. Nature *442*, 997–1002. https://doi.org/10.1038/nature05010.

44. Nowak, E.C., Weaver, C.T., Turner, H., Begum-Haque, S., Becher, B., Schreiner, B., Coyle, A.J., Kasper, L.H., and Noelle, R.J. (2009). IL-9 as a mediator of Th17-driven inflammatory disease. J. Exp. Med. *206*, 1653–1660. https://doi.org/10.1084/jem.20090246.

45. Turner, J.E., Morrison, P.J., Wilhelm, C., Wilson, M., Ahlfors, H., Renauld, J.C., Panzer, U., Helmby, H., and Stockinger, B. (2013). IL-9-mediated survival of type 2 innate lymphoid cells promotes damage control in helminth-induced lung inflammation. J. Exp. Med. *210*, 2951–2965. https://doi.org/10.1084/jem.20130071.

46. Kaplan, M.H. (2017). The transcription factor network in Th9 cells. Semin. Immunopathol. *39*, 11–20. https://doi.org/10.1007/s00281-016-0600-2.

47. Lu, Y., Hong, S., Li, H., Park, J., Hong, B., Wang, L., Zheng, Y., Liu, Z., Xu, J., He, J., et al. (2012). Th9 cells promote antitumor immune responses in vivo. J. Clin. Invest. *122*, 4160–4171. https://doi.org/10.1172/JCI65459.

48. Lu, Y., Wang, Q., Xue, G., Bi, E., Ma, X., Wang, A., Qian, J., Dong, C., and Yi, Q. (2018). Th9 cells represent a unique subset of CD4(+) T cells endowed with the ability to eradicate advanced tumors. Cancer Cell *33*, 1048–1060.e7. https://doi.org/10.1016/j.ccell.2018.05.004.

49. Purwar, R., Schlapbach, C., Xiao, S., Kang, H.S., Elyaman, W., Jiang, X., Jetten, A.M., Khoury, S.J., Fuhlbrigge, R.C., Kuchroo, V.K., et al. (2012). Robust tumor immunity to melanoma mediated by interleukin-9-producing T cells. Nat. Med. *18*, 1248–1253. https://doi.org/10.1038/nm.2856.

50. Gerlach, K., Hwang, Y., Nikolaev, A., Atreya, R., Dornhoff, H., Steiner, S., Lehr, H.A., Wirtz, S., Vieth, M., Waisman, A., et al. (2014). TH9 cells that express the transcription factor PU.1 drive T cell-mediated colitis via IL-9 receptor signaling in intestinal epithelial cells. Nat. Immunol. *15*, 676–686. https://doi.org/10.1038/ni.2920.

51. Nalleweg, N., Chiriac, M.T., Podstawa, E., Lehmann, C., Rau, T.T., Atreya, R., Krauss, E., Hundorfean, G., Fichtner-Feigl, S., Hartmann, A., et al. (2015). IL-9 and its receptor are predominantly involved in the pathogenesis of UC. Gut *64*, 743–755. https://doi.org/10.1136/gutjnl-2013-305947.

52. Angkasekwinai, P., and Dong, C. (2021). IL-9-producing T cells: potential players in allergy and cancer. Nat. Rev. Immunol. *21*, 37–48. https://doi.org/10.1038/s41577-020-0396-0.

53. Ma-Krupa, W., Jeon, M.S., Spoerl, S., Tedder, T.F., Goronzy, J.J., and Weyand, C.M. (2004). Activation of arterial wall dendritic cells and breakdown of self-tolerance in giant cell arteritis. J. Exp. Med. *199*, 173–183. https://doi.org/10.1084/jem.20030850.

54. Stanko, K., Iwert, C., Appelt, C., Vogt, K., Schumann, J., Strunk, F.J., Ahrlich, S., Schlickeiser, S., Romagnani, C., Jürchott, K., et al. (2018). CD96 expression determines the inflammatory potential of IL-9-producing Th9 cells. Proc. Natl. Acad. Sci. USA *115*, E2940–E2949. https://doi.org/10.1073/pnas.1708329115.

55. Chauvin, J.M., Pagliano, O., Fourcade, J., Sun, Z., Wang, H., Sander, C., Kirkwood, J.M., Chen, T.h.T., Maurer, M., Korman, A.J., and Zarour, H.M. (2015). TIGIT and PD-1 impair tumor antigen-specific CD8(+) T cells in melanoma patients. J. Clin. Invest. *125*, 2046–2058. https://doi.org/10.1172/JCI80445.

56. Joller, N., Hafler, J.P., Brynedal, B., Kassam, N., Spoerl, S., Levin, S.D., Sharpe, A.H., and Kuchroo, V.K. (2011). Cutting edge: TIGIT has T cell-intrinsic inhibitory functions. J. Immunol. *186*, 1338–1342. https://doi.org/10.4049/jimmunol.1003081.

57. Stanietsky, N., Simic, H., Arapovic, J., Toporik, A., Levy, O., Novik, A., Levine, Z., Beiman, M., Dassa, L., Achdout, H., et al. (2009). The interaction of TIGIT with PVR and PVRL2 inhibits human NK cell cytotoxicity. Proc. Natl. Acad. Sci. USA *106*, 17858–17863. https://doi.org/10.1073/pnas.0903474106.

58. Chiang, E.Y., de Almeida, P.E., de Almeida Nagata, D.E., Bowles, K.H., Du, X., Chitre, A.S., Banta, K.L., Kwon, Y., McKenzie, B., Mittman, S., et al. (2020). CD96 functions as a co-stimulatory receptor to enhance CD8(+) T cell activation and effector responses. Eur. J. Immunol. *50*, 891–902. https://doi.org/10.1002/eji.201948405.

59. Dougall, W.C., Kurtulus, S., Smyth, M.J., and Anderson, A.C. (2017). TIGIT and CD96: new checkpoint receptor targets for cancer immunotherapy. Immunol. Rev. *276*, 112–120. https://doi.org/10.1111/imr.12518.

60. Mueller, S., Cao, X., Welker, R., and Wimmer, E. (2002). Interaction of the poliovirus receptor CD155 with the dynein light chain Tctex-1 and its implication for poliovirus pathogenesis. J. Biol. Chem. *277*, 7897–7904. https://doi.org/10.1074/jbc.M111937200.

61. Zitti, B., Molfetta, R., Fionda, C., Quatrini, L., Stabile, H., Lecce, M., de Turris, V., Ricciardi, M.R., Petrucci, M.T., Cippitelli, M., et al. (2017). Innate immune activating ligand SUMOylation affects tumor cell recognition by NK cells. Sci. Rep. *7*, 10445. https://doi.org/10.1038/s41598-017-10403-0.

62. Zhang, H., Watanabe, R., Berry, G.J., Tian, L., Goronzy, J.J., and Weyand, C.M. (2018). Inhibition of JAK-STAT signaling suppresses pathogenic immune responses in medium and large vessel vasculitis. Circulation *137*, 1934–1948. https://doi.org/10.1161/CIRCULATIONAHA.117.030423.

63. Stamm, H., Klingler, F., Grossjohann, E.M., Muschhammer, J., Vettorazzi, E., Heuser, M., Mock, U., Thol, F., Vohwinkel, G., Latuske, E., et al. (2018). Immune checkpoints PVR and PVRL2 are prognostic markers in AML and their blockade represents a new therapeutic option. Oncogene *37*, 5269–5280. https://doi.org/10.1038/s41388-018-0288-y.

64. Watanabe, R., Shirai, T., Namkoong, H., Zhang, H., Berry, G.J., Wallis, B.B., Schaefgen, B., Harrison, D.G., Tremmel, J.A., Giacomini, J.C., et al. (2017). Pyruvate controls the checkpoint inhibitor PD-L1 and suppresses T cell immunity. J. Clin. Invest. *127*, 2725–2738. https://doi.org/10.1172/JCI92167.

STAR★METHODS

KEY RESOURCES TABLE

REAGENT or RESOURCE	SOURCE	IDENTIFIER
Antibodies		
mouse IgG	BioLegend	400124
mouse IgG	Thermo Fisher Scientific	02–6502
Alexa Fluor 594-mouse IgG	Thermo Fisher Scientific	A-11032
PE-mouse IgG	Thermo Fisher Scientific	P-852
FITC-rabbit IgG	abcam	ab97050
Alexa Fluor 488-rabbit IgG	Thermo Fisher Scientific	A-11008
CD3	Dako	A0452
FITC-CD3	BioLegend	344804
FITC-CD4	BioLegend	300506
FITC-CD4	BioLegend	357406
BV480-CD8	BD Biosciences	566121
FITC-CD14	BioLegend	325604
BV650-CCR7	BioLegend	353234
PE-Cy7-CD45	BioLegend	368532
BV570-CD45RA	BioLegend	304132
CD68	Thermo Fisher Scientific	PA5-32331
CD68	Cell Signaling Technology	76437
CD96	Thermo Fisher Scientific	PA5-97568
CD96	BioLegend	338402
PE-CD96	BioLegend	338406
BV421-CD96	BioLegend	338418
PE-PD-1	BioLegend	329906
PE/Dazzle594-TIGIT	BioLegend	372716
BV711-CD226	BioLegend	338334
PE/Cy5-TIM3	BioLegend	345052
PE/Cy7-LAG3	Thermo Fisher Scientific	25-2239-42
CD155	Thermo Fisher Scientific	MA5-13493
CD155	BioLegend	337502
CD155	Thermo Fisher Scientific	MA5-29762
PE-CD155	BioLegend	337507
CD63	Santa Cruz Biotechnology	sc-5275
GM130	abcam	ab52649
ERGIC-53/p58	Sigma	E1031
LAMP2A	abcam	ab18528
Calnexin	ABclonal	A15631
EEA1	ABclonal	A0592
LC3	MBL	PM036
HSP60	Santa Cruz Biotechnology	sc-13115
PerCP/Cy5.5-IFN-γ	BioLegend	502526
IL-9	BioLegend	507704
IL-9	proteintech	66144-1-Ig
BV421-IL-9	BD Biosciences	564254

(*Continued on next page*)

Continued

REAGENT or RESOURCE	SOURCE	IDENTIFIER
Biological samples		
PBMC	Stanford University School of Medicine/Mayo Clinic	N/A
Chemicals, peptides, and recombinant proteins		
Dynabeads Human T-Activator CD3/CD28	Thermo Fisher Scientific	11132D
Lymphoprep	Cosmo Bio USA	AXS-1114547
M-CSF	BioLegend	574806
IFN-γ	Sino Biological	11725
LPS	MilliporeSigma	L2630
Accutase Cell Detachment Solution	Innovative Cell Technologies	AT-104
DAPI	Thermo Fisher Scientific	D1306
Critical commercial assays		
EasySep™ Human Monocyte Enrichment Kit	Stemcell Technologies	19058
EasySep™ human naive CD4 T cell isolation kit	Stemcell Technologies	19555
EasySep™ human CD4 T cell isolation kit	Stemcell Technologies	17952
Experimental models: Organisms/strains		
NOD.Cg-Prkdc^{scid} Il2rg^{tm1Wjl}/SzJ (NSG) mice	The Jackson Laboratory	IMSR_JAX:005557
Oligonucleotides		
CD96 siRNA	horizon	L-020045-02-0005
control siRNA	horizon	D-001810-01-05
CD96 siRNA	Santa Cruz Biotechnology	sc-45460
control siRNA	Santa Cruz Biotechnology	sc-37007
Software and algorithms		
ZEN Software	Carl Zeiss	RRID:SCR_018163
FlowJo Flow Cytometry Analysis FlowJo	FlowJo	RRID:SCR_00852
ImageJ	ImageJ	RRID:SCR_003070
Prism Software	GraphPad	RRID:SCR_002798

RESOURCE AVAILABLITY

Lead contact

Further information and requests for resources and reagents should be directed to and will be fulfilled by the lead contact, Cornelia M. Weyand (cweyand@stanford.edu).

Materials availability

This study did not generate new unique reagents.

Data and code availability

- Data: The data that support the plots within this paper and other findings of this study are available from the lead contact upon request.
- Code: This paper does not report original code.
- General Statement: Any additional information required to reanalyze the data reported in this work paper is available from the lead contact upon request.

EXPERIMENTAL MODEL AND SUBJECT DETAILS

Patients and tissues

144 GCA patients with typical histological findings of GCA on temporal artery biopsy were enrolled into the study. Demographic characteristics of the patient population are summarized in Table S1. Demographically matched healthy subjects without any history of cancer, autoimmune disease, or chronic viral infection were recruited from the blood banks of Stanford University and Mayo Clinic Rochester (n = 145). Patients with a diagnosis of ANCA-positive granulomatosis with polyangiitis (GPA) were enrolled as disease controls.

Temporal arteries were collected from diagnostic biopsies of individuals suspected to have vasculitis. Serial sections of all biopsies were assessed for the presence of inflammatory cells, fragmentation of elastic laminae, and thickening of the adventitial and intimal layers. A diagnosis of vasculitis required unequivocal evidence for mononuclear cells infiltrating the vessel wall combined with damage to the wall structure. Nasal and sinal tissues were collected from diagnostic biopsies in patients suspected to have GPA. Normal human aorta, axillary and temporal arteries were donated by organ donors and harvested within 12 h postmortem.

The Institutional Review Board approved all bio-specimen collections and all procedures; written informed consent was obtained from all participants as appropriate. The Animal Care and Use Committee reviewed and approved all aspects of the animal protocol.

Cell preparation and culture

Peripheral blood mononuclear cells (PBMCs) were isolated from the peripheral blood of healthy individuals and patients by density gradient centrifugation with Lymphoprep (#AXS-1114547; Cosmo Bio USA, CA, United States). Monocytes isolated from PBMCs were isolated with EasySep Human Monocyte Enrichment Kit (#19058; Stemcell Technologies), or by plastic adherence as previously described.[19] Monocytes were differentiated into Mφ by treatment with 20 ng/mL macrophage-CSF (M-CSF) (#574806; BioLegend, CA, United States) for 5-day as reported.[19] Mφ were further differentiated by stimulating with 100 U/mL IFN-γ (#11725-HNAS; Sino Biological; PA, United States) and 100 ng/mL LPS (#L2630; MilliporeSigma, MA, United States). Mφ were detached from plates using Accutase Cell Detachment Solution (#AT-104; Innovative Cell Technologies, CA, United States) and Cell Scraper (#3010; Corning, NY, United States). Naive CD4 T cells and total CD4 T cells were purified using the EasySep human naive CD4 T cell and human CD4 T cell isolation kits (#19555, #17952; Stemcell Technologies, Vancouver, Canada). Cells were cultured in RPMI 1640 medium (#11875135; Thermo Fisher Scientific, MA, United States) supplemented with 10% FBS (#100–106; GeminiBio, CA, United States) and were incubated at 37°C with 5% CO_2.

Human artery-severe combined immunodeficiency mouse chimeras

NOD.Cg-Prkdc^{scid} Il2rg^{tm1Wjl}/SzJ (NSG) mice were purchased from the Jackson Laboratory (IMSR_JAX:005557; Sacramento, CA) and chimeras were generated as previously described.[5,16,62] Randomly selected male and female mice were used in this study at the age of 6–10 weeks. Non-inflamed human temporal or axillary arteries were engrafted subcutaneously into the back of the NSG mice.[5,16,62] Seven days after the engraftment, PBMC from GCA patients were adoptively transferred into the chimeras (10–20 million cells per mouse). Chimeras were randomly assigned to 2–3 treatment arms in each experiment. Engrafted arteries were harvested on day 21 and shock-frozen for RNA isolation or embedded into OCT for H&E staining or immunostaining.

For gain-of-function and loss-of-function experiments, anti-human IL-9 (100 μg, #507704, BioLegend), isotype control IgG (100 μg, #400124, BioLegend), human recombinant IL-9 (200 ng, #11844-H08B-5, Sino Biological), or saline were injected intraperitoneally every other day for one week. CD96 was knocked down by siRNA technology. CD4 T cells were isolated from GCA patients and transfected with siRNA using the Amaxa Nucleofector system and the Human Nucleofector kit (Lonza). CD96 siRNA-transfected T cells were recombined with autologous T cell-depleted peripheral mononuclear cells and adoptively transferred into chimeric mice to induce vasculitis (total 10–20 million cells per mouse). To extract T cells from the inflamed arteries, explanted tissues were minced and shaken at 37 °C, 100 rpm, for 1 h with 1.5 mg/mL collagenase I (#LS004196; Worthington Biochemical Corporation, NJ, United States) and 100 μg/mL DNase I (#E1011-A; Zymo Research, CA, United States) in HBSS (#14025076; Thermo Fisher Scientific). Cells were filtered to prepare single-cell suspensions using 35 μm filters.

METHOD DETAILS

Macrophage-T cell co-cultures

PBMC-derived monocytes from patients with GCA or healthy donor were isolated using the EasySep Human Monocyte Enrichment Kit (#19058; Stemcell Technologies). 10,000 cells were seeded with M-CSF, cultured for 5-day in 96-well plates, and stimulated with IFN-γ/LPS for 24-h as described above. After stimulation, monocyte derived Mφ were loaded with 1.5 μg/mL anti-CD3/OKT antibody (BioLegend) as previously desribed[19] and co-cultured with 50,000 isolated naive CD4 T cells from healthy individuals for 72 h. Antibody-blocking experiments with anti-CD155 antibody (Thermo Fisher Scientific), anti-CD96 antibody (BioLegend), or isotype control antibodies (Thermo, Biolegend) followed previously described protocols.[63]

Quantitative reverse transcription polymerase chain reaction (RT-PCR)

Methods for RNA isolation, reverse transcription and quantitative PCR have been published.[16,64] Gene transcript numbers were adjusted relative to β-actin transcripts. Primers are listed in Table S2.

Flow cytometry and multiparametric phenotyping

Expression of surface molecules was analyzed using the BD LSRFortessa (BD Biosciences, CA, USA) or the CYTEK Aurora (Cytek Biosciences, CA, United States). Data analysis followed the workflow in FlowJo (Tree Star, OR, United States). Cells were stained with diluted antibodies, and Zombie NIR (#423106, BioLegend) was used to distinguish live/dead cells. Staining was performed in wash buffer (BD Biosciences) for 30 min at 4 °C. For multiparametric assays, after exclusion of dead cell by Zombie NIR staining, memory T cells were gated based on expression of CD45RA and CCR7. Using FlowJo software, dimensionality reduction was

performed applying uniform manifold approximation and projection (UMAP). FlowJo plugin Phenograph was used for the identification of unique cell populations (cluster) on the resulting UMAP map. Quantified frequencies of each cluster are presented as pie charts. To evaluate intracellular cytokine production, cells were treated with Cell Activation Cocktail (#423301, BioLegend) for 6 h, permeabilized using the BD Cytofix/Cytoperm Kit (#554714, BD Biosciences), stained with specific antibodies, and analyzed by flow cytometry. GolgiStop (#554724, BD Biosciences) was added at the same time to inhibit protein release to the extracellular space. The antibodies used in flow cytometry experiments are listed in Table S3.

Immunohistochemistry and immunofluorescence

Tissues were shock-frozen in OCT on dry ice and blocks stored in −80°C as described.[5,62] Five-micron sections were fixed with precold acetone for 15 min and incubated with 0.3% H_2O_2 buffer for 15 min at room temperature. For dual-color immunohistochemistry, tissue sections were stained with primary antibodies. Bound antibodies were visualized with anti-rabbit or anti-mouse secondary antibodies. Tissues were counterstained with DAPI (#D1306, Thermo Fisher Scientific) and images were taken with an Olympus fluorescence microscopy system (Olympus, Tokyo, Japan). Tissues stained with anti-CD96 or anti-CD155 antibodies were analyzed by the All-in-One Fluorescence Microscope BZX800E system (Keyence, Kyoto, Japan) and Zeiss LSM780 confocal microscope (Zeiss, Oberkochen, Germany). The antibodies used in immunohistochemistry are listed in Table S2.

QUANTIFICATION AND STATISTICAL ANALYSIS

All analyses were performed using Prism9 (Version 9.5.0; GraphPad Software, La Jolla, CA). Statistical significance was assessed by unpaired or paired 2-tailed Student's *t* test (parametric), Mann-Whitney U test or Wilcoxon test (nonparametric), or one-way analysis of variance (ANOVA) with post hoc Tukey's multiple comparisons test (3 or more groups). The number of samples used in the analysis, the method of analysis, and the meaning of the bar graphs are described in the legend of each figure.

Cell Reports Medicine, Volume *4*

Supplemental information

Deficiency of the CD155-CD96 immune checkpoint controls IL-9 production in giant cell arteritis

Shozo Ohtsuki, Chenyao Wang, Ryu Watanabe, Hui Zhang, Mitsuhiro Akiyama, Melanie C. Bois, Joseph J. Maleszewski, Kenneth J. Warrington, Gerald J. Berry, Jörg J. Goronzy, and Cornelia M. Weyand

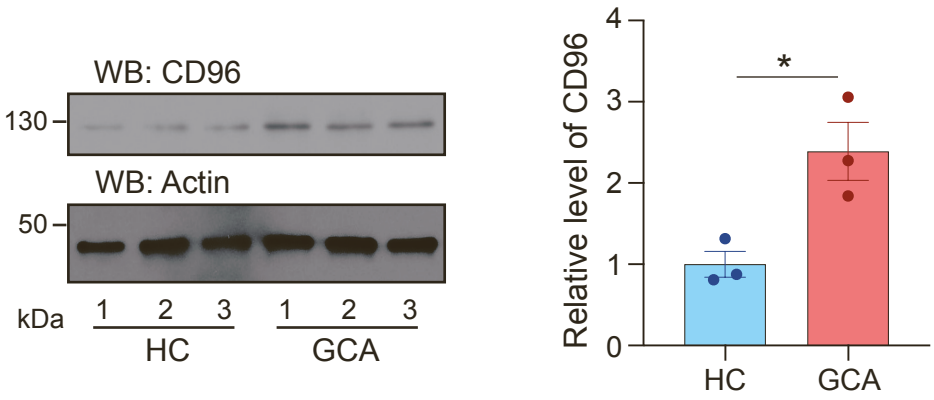

Supplemental Figure S1. Accumulation of CD96^{high} CD4^{+} T cells in GCA patients.

Immunoblotting of CD96 protein in control and patient-derived resting CD4^{+} T cells. b-actin served as a control. Bar graph shows protein quantification. Data from 3 GCA patients and 3 healthy controls.
Two-tailed unpaired t test. *<0.05.

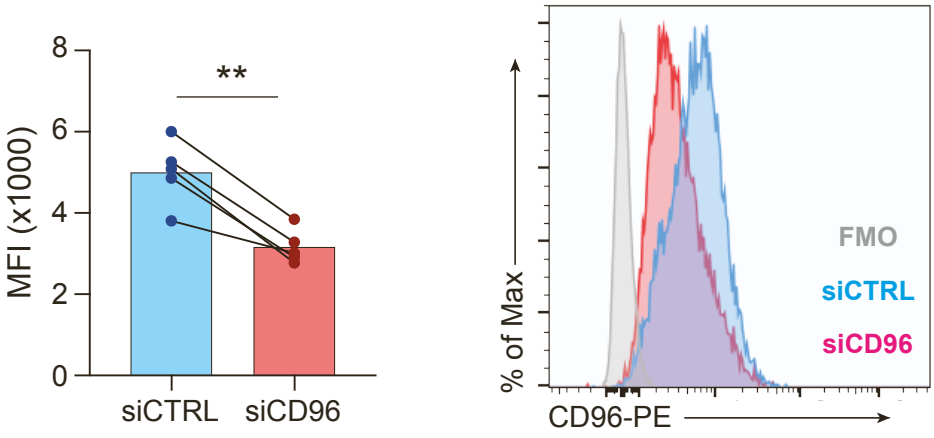

Supplemental Figure S2. Knockdown efficiency for CD96.

CD96 was knocked down by transfecting $CD4^+$ T cells with CD96-specific or control siRNA. CD96 protein expression was quantified by FACS (n=5). Two-tailed paired t test. **<0.01.

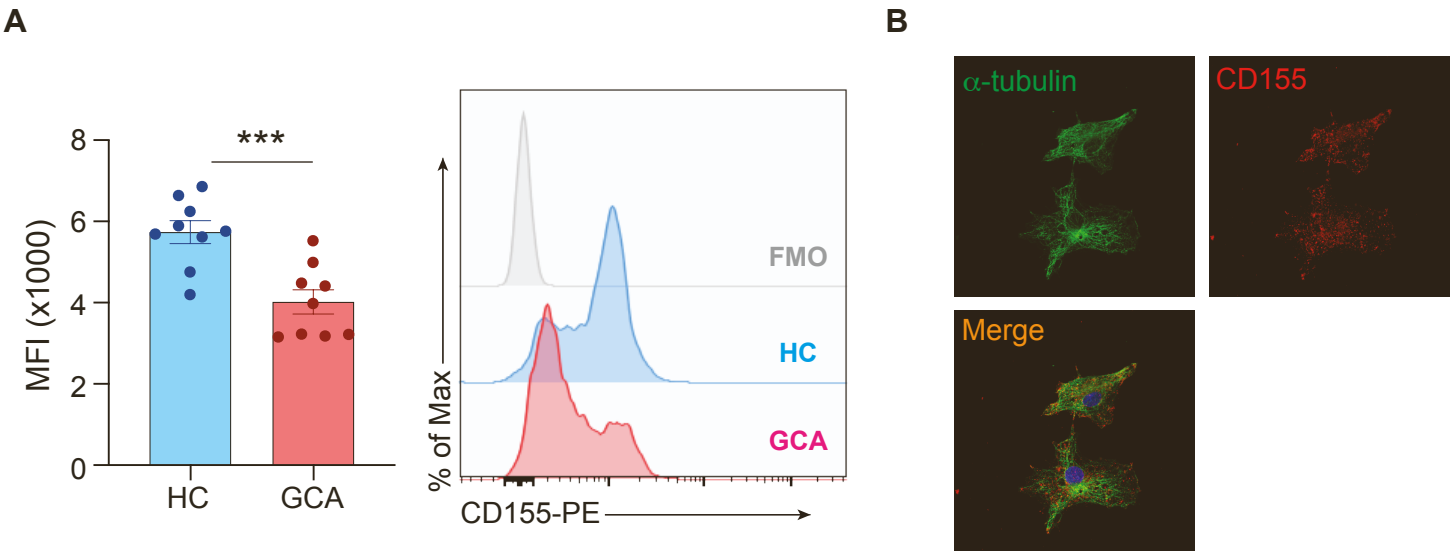

Supplemental Figure S3. CD155 low-expressing monocytes in giant cell arteritis (GCA).

(A) Flow cytometric analysis of CD155 expression on $CD14^+$ monocytes from GCA patients and age-matched controls. Representative histograms and MFI are shown. Each dot represents one patient or one healthy individual.
(B) Monocyte-derived macrophages were induced from GCA patients and stained for CD155 (red) and α-tubulin (green) as structure marker.
Two-tailed unpaired t test. ***<0.001

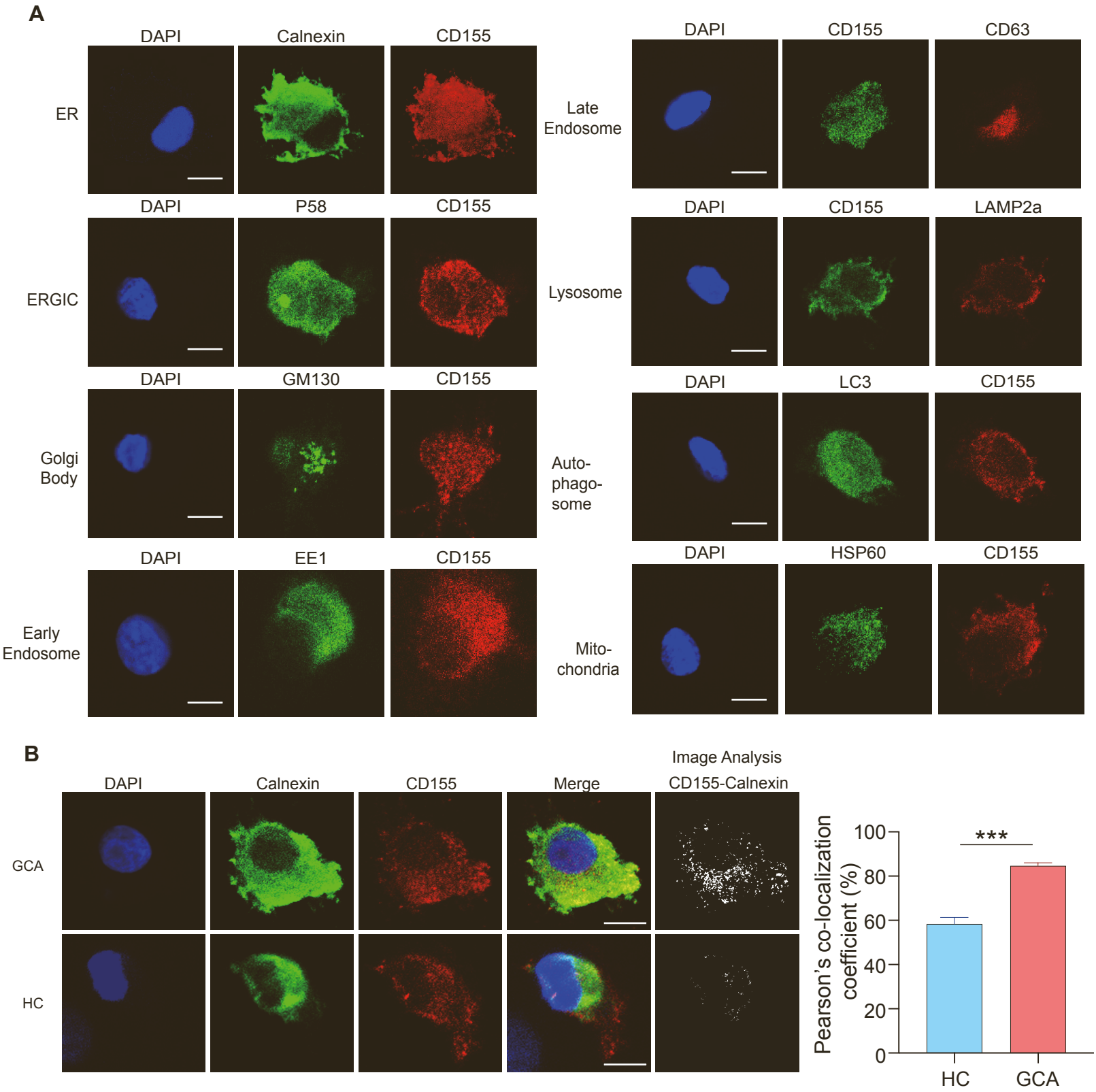

Supplemental Figure S4. GCA macrophages under ER stress trap CD155 in the cytoplasm.

Monocyte-derived macrophages were generated from age-matched controls and GCA patients and stimulated with LPS/IFN-γ.
(A) Macrophages were stained for CD155 and cellular organelles and imaged by fluorescence microscopy. Markers represent the following organelles: (Calnexin; ER), (P58; ERGIC), (GM130; Golgi body), (EE1; early endosome), (CD63; late endosome), (LAMP2a; lysosome), (LC3; autophagosome), (HSP60; mitochondria), (DAPI; nucleus).
(B) HC macrophages and GCA macrophages were stained for CD155 and Calnexin. Cellular stains were analyzed by imaging software to reveal co-localization as white dots (right panel). Scale bar; 5 μm. Representative images for each subcellular organelle are shown.

Supplemental Table 1. Clinical characteristics of patients with giant cell arteritis

Parameters	Patients (n=144)
Age (year, mean ± SD)	73.60 ± 8.70
Female	101 (70.1%)
Ethnicity	
Caucasian	121 (84.0%)
African American	6 (4.2%)
Hispanic	8 (5.6%)
Asian	6 (4.2%)
Other	3 (2.1%)
Disease Duration (months, mean ± SD)	6.31 ± 7.86
Erythrocyte sedimentation rate (mean ± SD, mm/h)	36.76 ± 27.81
C-reactive protein (mean ± SD, mg/dL)	7.94 ± 13.95
Headaches	70 (48.6%)
Eye involvement	50 (34.7%)
Aortic/large vessel involvement	84 (58.3%)
Polymyalgia rheumatica	92 (63.9%)
Treatment of GCA	
Untreated	44 (30.6%)
Prednisone (mg/day, mean ± SD)	5.17 ± 7.47
Second immunosuppressant	37 (25.7%)

Supplemental Table 2. PCR primers used in this study

Genes	Forward	Reverse
β-actin	GATCATTGCTCCTCCTGAGC	CGTCATACTCCTGCTTGCTG
IL-1β	AAGTACTGAGCTCGCCAGTGAAA	TTGCTGTAGTGGTGGTCGGAGATT
IL-2	AACTCCTGTCTTGCATTGCAC	GCTCCAGTTGTAGCTGTGTTT
IL-4	TACAGCCACCATGAGAAGGACACT	TTCCTGTCGAGCCGTTTCAGGAAT
IL-5	TGGAGCTGCCTACGTGTATG	TTCGATGAGTAGAAAGCAGTGC
IL-6	AGCCACTCACCTCTTCAGAACGAA	AGTGCCTCTTTGCTGCTTTCACAC
IL-9	GGGATCCTGGACATCAACTTC	GAAGCATGGTCTGGTGCAGTT
IL-9	CTCTGTTTGGGCATTCCCTCT	GGGTATCTTGTTTGCATGGTGG
IL-10	TCCTTGCTGGAGGACTTTAAGGGT	TGTCTGGGTCTTGGTTCTCAGCTT
IL-13	CAACGCTCATTGCTCTCACTTGCC	CCTTGTGCGGGCAGAATCCGCTCA
IL-17A	AACCGATCCACCTCACCTTGGAAT	TTCATGTGGTAGTCCACGTTCCCA
IL-18	TCTTCATTGACCAAGGAAATCGG	TCCGGGGTGCATTATCTCTAC
IL-21	TCCTGGCAACATGGAGAGGATTGT	AGCTGGCAGAAATTCAGGGACCAA
IL-22	CCTATATCACCAACCGCACCTTC	AGATTGAGGGAACAGCACTTCTTC
IL-9 receptor	GCAACATCAGTTCTGGCCCAC	TGCTTCCAGGCTCCCCGA
IFN-γ	ACTAGGCAGCCAACCTAAGCAAGA	CATCAGGGTCACCTGACACATTCA
TNF-α	GGTGGTGCCATCAGAGGGCC	GAGCACATGGGTGGAGGGGC
TNF-α	GGGACCTCTCTCTAATCAGCC	GTTATCTCTCAGCTCCACGCC
GM-CSF	GGGAGCATGTGAATGCCATC	GGCTCCTGGAGGTCAAACAT
TGF-β	ACTTGCACCACCTTGGACTTC	GGTCATCACCGTTGGCTCA
T cell receptor	CCTTCAACAACAGCATTATTATTCCAG	CGAGGGAGCACAGGCTGTCTTA
CD80	ATGGTGGGCACAGAAGTAGC	AGGAAATCTGGGTTCTGGCG
CD86	TGGTCAGGGAGGGGTTTTGG	GCCCCGGGTGATCTGTGTCT
CD96	CAAACACAGACAGTAGGCTTCTT	GGGGATGATAGACAGCAATCAG
CD155	TGGAGGTGACGCATGTGTC	GTTTGGACTCCGAATAGCTGG
ATF4	ATGACCGAAATGAGCTTCCTG	GCTGGAGAACCCATGAGGT
ATF6	TCCTCGGTCAGTGGACTCTTA	CTTGGGCTGAATTGAAGGTTTTG
BiP	GAAAGAAGGTTACCCATGCAGT	CAGGCCATAAGCAATAGCAGC
CHOP	GGAAACAGAGTGGTCATTCCC	CTGCTTGAGCCGTTCATTCTC
TRIB3	AAGCGGTTGGAGTTGGATGAC	CACGATCTGGAGCAGTAGGTG
XBP1	CCCTCCAGAACATCTCCCCAT	ACATGACTGGGTCCAAGTTGT

Supplemental Table 3. Antibodies used in this study

Antigen	Conjugated	Source	Catalog No
Control mouse IgG	None	BioLegend	400124
Control mouse IgG	None	Thermo Fischer Scientific	02-6502
Mouse IgG	Alexa Fluor 594	Thermo Fisher Scientific	A-11032
Mouse IgG	PE	Thermo Fisher Scientific	P-852
Rabbit IgG	FITC	abcam	ab97050
Rabbit IgG	Alexa Fluor 488	Thermo Fisher Scientific	A-11008
CD3	None	Dako	A0452
CD3	FITC	Biolegend	344804
CD4	FITC	BioLegend	300506
CD4	FITC	BioLegend	357406
CD8	BV480	BD Biosciences	566121
CD14	FITC	BioLegend	325604
CCR7	BV650	Biolegend	353234
CD45	PE-Cy7	BioLegend	368532
CD45RA	BV570	Biolegend	304132
CD68	None	Thermo Fisher Scientific	PA5-32331
CD68	None	Cell Signaling Technology	76437
CD163	None	Thermo Fisher Scientific	MA5-11458
CD96	None	Thermo Fisher Scientific	PA5-97568
CD96	None	BioLegend	338402
CD96	PE	BioLegend	338406
CD96	BV421	Biolegend	338418
PD-1	PE	Biolegend	329906
TIGIT	PE/Dazzle594	Biolegend	372716
CD226	BV711	Biolegend	338334
TIM3	PE/Cy5	Biolegend	345052
LAG3	PE/Cy7	Thermo Fischer Scientific	25-2239-42
CD155	None	Thermo Fischer Scientific	MA5-13493
CD155	None	BioLegend	337502
CD155	None	Thermo Fischer Scientific	MA5-29762
CD155	PE	BioLegend	337507
CD63	None	Santa Cruz Biotechnology	sc-5275
GM130	None	abcam	ab52649
ERGIC-53/p58	None	Sigma	E1031
LAMP2A	None	abcam	ab18528
Calnexin	None	Abclonal	A15631
ee1	None	Abclonal	A0592
LC3	None	MBL	PM036
HSP60	None	Santa Cruz Biotechnology	sc-13115
GRP78	None	Thermo Fischer Scientific	PA1-014A
IFN-γ	PerCP/Cy5.5	BioLegend	502526
IL-9	None	BioLegend	507704
IL-9	None	proteintech	66144-Ig
IL-9	BV421	BD Bioscience	564254